(4)

TECHNICAL REPORT BRL-TR-2977

BRL

1938 – Serving the Army for Fifty Years – 1988

ANALYSIS OF TURBULENT BOUNDARY-LAYER OVER ROUGH SURFACES WITH APPLICATION TO PROJECTILE AERODYNAMICS

JAMES E. DANBERG
ASHER SIGAL

DECEMBER 1988

U.S. ARMY LABORATORY COMMAND

BALLISTIC RESEARCH LABORATORY
ABERDEEN PROVING GROUND, MARYLAND

DESTRUCTION NOTICE

Destroy this report when it is no longer needed. DO NOT return it to the originator.

Additional copies of this report may be obtained from the National Technical Information Service, U.S. Department of Commerce, Springfield, VA 22161.

The findings of this report are not to be construed as an official Department of the Army position, unless so designated by other authorized documents.

The use of trade names or manufacturers' names in this report does not constitute indorsement of any commercial product.

REPORT DOCUMENTATION PAGE

Form Approved OMB No. 0704-0188

1a. REPORT SECURITY CLASSIFICATION: UNCLASSIFIED	1b. RESTRICTIVE MARKINGS
2a. SECURITY CLASSIFICATION AUTHORITY	3. DISTRIBUTION/AVAILABILITY OF REPORT: Approved for public release, distribution unlimited.
2b. DECLASSIFICATION/DOWNGRADING SCHEDULE	
4. PERFORMING ORGANIZATION REPORT NUMBER(S): BRL-TR-2977	5. MONITORING ORGANIZATION REPORT NUMBER(S)
6a. NAME OF PERFORMING ORGANIZATION: U.S. Army Ballistic Research Laboratory; 6b. OFFICE SYMBOL (If applicable): SLCBR-LF	7a. NAME OF MONITORING ORGANIZATION
6c. ADDRESS (City, State, and ZIP Code): Aberdeen Proving Ground, Maryland 21005-5066	7b. ADDRESS (City, State, and ZIP Code)
8a. NAME OF FUNDING/SPONSORING ORGANIZATION; 8b. OFFICE SYMBOL (If applicable)	9. PROCUREMENT INSTRUMENT IDENTIFICATION NUMBER
8c. ADDRESS (City, State, and ZIP Code)	10. SOURCE OF FUNDING NUMBERS: PROGRAM ELEMENT NO. 62618A; PROJECT NO. 1L162618AH80; TASK NO. 00; WORK UNIT ACCESSION NO. 001 AJ

11. TITLE (Include Security Classification)
ANALYSIS OF TURBULENT BOUNDARY-LAYER OVER ROUGH SURFACES WITH APPLICATION TO PROJECTILE AERODYNAMICS

12. PERSONAL AUTHOR(S)
SIGAL, ASHER* and DANBERG, JAMES E.

13a. TYPE OF REPORT	13b. TIME COVERED	14. DATE OF REPORT (Year, Month, Day)	15. PAGE COUNT
Technical Report	FROM _____ TO _____		

16. SUPPLEMENTARY NOTATION
*Associate Projessor of Aeronautics, Technion, Department of Aeronautical Engineeringing, Technion City, Haifa 32000, Israel

17. COSATI CODES			18. SUBJECT TERMS (Continue on reverse if necessary and identify by block number)
FIELD	GROUP	SUB-GROUP	
01	01		Turbulent Boundary Layer Rough Wall

19. ABSTRACT (Continue on reverse if necessary and identify by block number)

A new correlation of the roughness density effect on the intercept of the law of the wall and the equivalent sand roughness, has been developed. The data base used includes corrected results of Schlichting's rough channel experiment and those of twelve other studies. The roughness density parameter used is a product of the reference surface to the total frontal area ratio and a shape factor. For two dimensional roughnesses, the new parameter correlates data for circular wires with that of square bars. For three-dimensional roughnesses, it correlates results from all four types of roughnesses studied by Schlichting. The effect of three-dimensional roughness is a little smaller than that of two-dimensional roughness, having the same density parameter.

A component build-up engineering analysis has been used to estimate the additional axial-force, due to grooves and threads, of projectiles. Comparison of this prediction technique
(Continued on reverse side of this form.)

20. DISTRIBUTION/AVAILABILITY OF ABSTRACT	21. ABSTRACT SECURITY CLASSIFICATION
☐ UNCLASSIFIED/UNLIMITED ☐ SAME AS RPT. ☐ DTIC USERS	UNCLASSIFIED

22a. NAME OF RESPONSIBLE INDIVIDUAL	22b. TELEPHONE (Include Area Code)	22c. OFFICE SYMBOL
James E. Danberg	(301) 278-6280	SLCBR-LF-C

19. ABSTRACT (Continued)

and wind-tunnel data shows good agreement. Because the groove roughness, in the case considered here, is beyond the range of applicability of the new correlation, existing data are used to estimate an equivalent sand roughness.

A turbulence model, based on that of Healzer and the equivalent sand roughness concept has been implemented in the Schiff and Steger PNS code. In order to numerically evaluate the conditions over a rough surface, a transition region between smooth and rough surfaces is introduced. This transition region allows the effect of the rough surface conditions to propagate into this viscous flow region in a realistic way. The predicted smooth body axial force coefficient, excluding the base drag, is five percent smaller than that measured in a wind tunnel test. The predicted increment in axial force coefficient, due to the buttress grooves, is smaller (17 percent in one case and 56 percent in another) then that obtained experimentally at a Mach number of 5.0.

TABLE OF CONTENTS

TABLE OF CONTENTS (continued)

LIST OF FIGURES

LIST OF FIGURES

I. INTRODUCTION

Many types of artillery projectiles are accelerated in the barrel by a sabot. The transfer of the accelerating force from the sabot to the projectile is accomplished by a series of threads or grooves in the later. These surfaces are referred to as buttress threads or grooves in the following. Aerodynamically, these mechanical engagement devices are roughness elements although the roughness heights can be large relative to the boundary layer thickness. They produce two effects: one is an increase in the axial force, and the other an increase in the thickness of the boundary layer which can result in an interaction with the rear end of the configuration. These effects may be significant, hence they must be included in the prediction of the aerodynamic characteristics of such projectiles. A shadowgraph of a typical high speed kinetic energy projectile in flight is shown in Figure 1 in which the buttress grooves and their effect on the boundary layer are evident.

The goal of this work is to review prediction methods for turbulent boundary layers over rough surfaces, with the objective of selecting the ones that best fit the ongoing activity of the Computational Aerodynamics Branch, Launch and Flight Division, US Army Ballistic Research Laboratory, (BRL) Aberdeen Proving Ground, Maryland, and then to implement and validate them.

Most roughness elements employed in ballistics are circumferential. From an aerodynamic point of view, they are two-dimensional. As a result, the search covers, mainly, investigations concerning two-dimensional roughness.

II. CLASSIFICATION OF PREDICTION METHODS

Prediction methods can be classified into two main approaches: 1) Correlation methodologies; and 2) Analytical predictive techniques. The first ones are based on existing experimental (or empirical) data and are useful as long as sufficient data are available under conditions reasonably close to the design problem. It is, however, of little help if the data are sparse or missing. Current activities at BRL include Mikhail's[1] correlation of available data on rough projectiles.

A classification tree of predictive methods is shown in Figure 2. The main methods for the analysis of boundary layers are: 1) integral methods; and 2) differential methods. Both classes have been successfully used for the case of turbulent boundary layers over rough surfaces. However, the differential methods can be modified more easily to handle the three-dimensional case of a configuration at an angle-of-attack and the case of the interaction between a body boundary-layer and stabilizing fins. Also, the differential methods have an advantage in the present work because they can be incorporated into existing numerical techniques and codes in the field of computational aerodynamics.

The differential methods can be divided into two major approaches: 1) distributed roughness; and 2) discrete element.

The foundation for the distributed roughness approach is the well established empirical relationship between sand-grain roughness and the skin friction and the velocity profile. For roughness other than that of sand grain, empirical data is used to find an equivalent sand-grain roughness. This approach will be elaborated on in the next Chapter.

The discrete element approach estimates the form drag and the heat transfer to the individual roughness elements. These quantities are added to the friction drag and the heat transfer to the smooth sections between the excrescences. This approach can be further divided into two branches, according to the grid used in the numerical solution: 1) micro grid; and 2) macro grid.

In the first case, the grid follows the actual surface. Thus, it has to be fine enough to describe the geometry and the turbulence quantities in detail. In principle, this approach will solve the complete (i.e., time dependent) Navier-Stokes equations or the time-averaged ones. This method was used recently by Sahu and Danberg[2] to study supersonic flow over a rotating band. Baysal and Stallings[3] studied flow over a cavity and Venkataphaty, et al[4] considered the flow over a two-dimensional groove having a square cross-section.

In spite of the demonstrated success, to date, this procedure has had application only in configurations having a small number of roughness elements. Many configurations, in the field of ballistics, have large series of roughness elements. In these cases, the computational requirements are beyond the present capacity of codes and machines.

The second branch, that of macro grid ignores the fine details of the flow near the wall. The actual surface is represented by a smooth one. The equations of motion are altered to account for the blocking effect of the protruberances; the estimated form drag of the discrete elements is taken into account in the momentum equation; the estimated heat transfer is taken into account by the energy equation. Hodge and Adams[5] used this approach for sand-grain roughness at supersonic and hypersonic Mach numbers. More recently, Taylor, et al[6] extended this approach for two-dimensional, rib-type roughness.

The following conclusions are made, based on the above overview: The micro grid branch has the greatest potential and is highly recommended because it requires the least specific empirical data. However, it is presently limited to configurations having only a small number of roughness elements. It is expected that the application of this branch will expand, as computing capacity grows in the future.

The main issue, for the analysis of configurations having many roughness elements is between the distributed roughness approach and the macro grid branch of the discrete element approach. The later introduces physical reasoning to the analysis. Nevertheless, it depends on empirical data and contains assumptions that need verification, especially for application to supersonic Mach numbers and dense roughness. At present, it does not provide an advantage over the other and more established methods. Hence the distributed roughness approach was selected for the present study.

III. SAND ROUGHNESS

1. REVIEW OF FUNDAMENTALS

It is commonly assumed, in the analysis of turbulent boundary layers, that Reynolds stresses dominate in the inner region, except for the wall layer. This assumption, together with similarity considerations, led to the well known Law of the Wall:

$$\frac{u}{u_\tau} = \frac{1}{\kappa} ln\frac{yu_\tau}{\nu} + C \quad . \tag{1}$$

Schlichting's[7] values for the Von Karman constant, κ, and the free constant, C, are 0.40 and 5.5, respectively. These values will be used in the present work.

Roughness elements, are a source of additional turbulent eddies near the wall. These eddies increase the Reynolds stresses in the wall layer. It is well established (e.g. Clauser,[8] Rotta[9]) that the effect of the additional stresses is a downward shift of the logarithmic velocity profile. The Law of the Wall for flow over rough surface becomes.

$$\frac{u}{u_\tau} = \frac{1}{\kappa} ln\frac{yu_\tau}{\nu} + C - \frac{\Delta u}{u_\tau} \quad . \tag{2}$$

The change of the intercept depends on the normalized roughness height, hu_τ/ν, the geometry of the roughness elements, their density and their arrangement on the wall.

2. EMPIRICAL DATA

The first and most quoted study of the effect of sand roughness on pipe flow is that of Nikuradse.[10] He validated the Law of the Wall for rough surfaces and proposed three regions of roughness

$$\frac{h_s u_\tau}{\nu} < 7 \quad : \text{ hydraulically smooth,}$$

$$7 < \frac{h_s u_\tau}{\nu} < 70 : \text{ intermediate rough,} \qquad (3)$$

$$70 < \frac{h_s u_\tau}{\nu} : \text{ fully rough.}$$

The dependence of the normalized displacement of the logarithmic velocity profile, relative to the smooth case, is shown in Figure 3. For the fully rough region it was found, based on Nikuradse's data, that

$$\frac{\Delta u}{u_\tau} = \frac{1}{\kappa} \ln \frac{h_s u_\tau}{\nu} - 3.0 \; . \qquad (4)$$

Goddard,[11] Fenter,[12] and Reda, et al[13] extended the data base to supersonic Mach numbers. Their results, concerning the displacement of the logarithmic velocity profile are shown in Figure 3, in comparison with those of Nikuradse. It is apparent that the displacement is independent of Mach number, provided the kinematic viscosity is evaluated at the wall.

The amplification in skin friction, which is the ratio of rough wall to smooth wall skin-friction coefficients, is shown in Figure 4. The following relationship has been found by the present authors to fit the data.

$$\frac{C_f}{C_{fo}} = 0.11 + 0.89 \log \frac{h_s u_\tau}{\nu_w} \; . \qquad (5)$$

IV. EQUIVALENT SAND ROUGHNESS

1. THE CONCEPT OF EQUIVALENT SAND ROUGHNESS

Three years after Nikuradse[10] obtained the data on flow in pipes roughened by closely packed sand grains, Schlichting[14,7] published results of measurements of the drag produced by other forms of roughness. His configurations were made of spheres, spherical segments, cones and short angles, arranged in regular patterns. Some configurations yielded more drag than that produced by sand roughness of the same height, while others gave drag that was smaller.

Schlichting proposed to consider sand-grain roughness as a standard and introduced the concept of equivalent sand roughness which is the size of sand grains that produce the same drag

as an actual configuration, under the same flow conditions. The range of the ratio of the size of the equivalent sand roughness to the height of the roughness elements in his test varied between 0.15 and 3.8, demonstrating the importance of the shape and the arrangement in determining the effect of roughness.

It is assumed that the wall velocity profile with actual roughness is the same as that for equivalent roughness. Introducing the index 'es' for equivalent sand, the condition for $C_f = C_{f_{es}}$ gives:

$$\frac{\Delta u}{u_\tau} = \left(\frac{\Delta u}{u_\tau}\right)_{es} . \tag{6}$$

In the region of fully rough flow:

$$\frac{\Delta u}{u_\tau} = \frac{1}{\kappa} ln\frac{hu_\tau}{\nu} + D . \tag{7}$$

Hence, the equivalent sand roughness can be obtained by:

$$\frac{1}{\kappa} ln\frac{hu_\tau}{\nu} + D = \frac{1}{\kappa} ln\frac{h_{es}u_\tau}{\nu} + D_S . \tag{8}$$

Introducing $D_s = -3.0$, as found by Nikuradse, and arranging:

$$\frac{h_{es}}{h} = \exp[\kappa(3.0 + D)] . \tag{9}$$

This relationship gives a means of determining the equivalent sand roughness, given the change in the intercept of the Law of the Wall.

2. REVIEW OF EXISTING CORRELATIONS

The effect of spacing on two-dimensional roughness was first studied by Morris.[15] He classified the flow fields into three types: skimming, wake-interference, and isolated roughness.

A pioneering attempt to quantify the effect of the spacing of two-dimensional roughness elements was performed by Bettermann[16] in 1965. For roughness composed of transverse square bars he correlated the change of the intercept by the relationship:

$$D = 17.55(1.634 \log \lambda_h - 1.0) \tag{10}$$

where the roughness density parameter is the pitch or wave length to height ratio, $\lambda_h = p/h$.

In 1969, Dvorak[17] introduced pitch to width ratio as a density of roughness elements parameter, $\lambda_a = p/a$. For parameter values less than about 5.0, and for square roughness, he corroborated Bettermann's correlation. For larger values, part of Schlichting's data and that of other sources, were used to establish a complementary correlation.

$$D = \begin{cases} 17.35(1.625 \log \lambda_a - 1.0) , & \lambda_a \leq 4.68 , \\ -5.95(1.103 \log \lambda_a - 1.0) , & \lambda_a > 4.68) . \end{cases} \qquad (11)$$

Note: The small difference between the constant multiplying log λ in Bettermann's article and that published later by Dvorak, is of little practical significance.

The above relationship between the displacement of the velocity profile and the density of the roughness was adopted by Cebeci and Smith[18] in their text on the analysis of turbulent boundary layers.

In 1973 Simpson[19] suggested a more general interpretation of the Bettermann and Dvorak correlation, by replacing their roughness density parameters by the ratio of reference area to total roughness frontal area. The reference area, S, is defined as the smooth surface before adding the roughness.

$$\lambda_f = \frac{S}{S_f} .$$

The rational for this generalization lays in the fact that for fully rough surfaces, the tangential forces are predominately due to form drag of the elements, which is proportional to their frontal area. By including additional data, he discovered two empirical findings. First, for low values of the density parameter two branches exist, depending on the formation or nonexistence of transverse vortices between rows of the roughness elements. Second, the shape of the roughness elements is an important parameter that should not be overlooked.

For the case of two-dimensional roughness, the Simpson interpretation of the density parameter is identical to that of Bettermann.

The two branches of the correlations represent two types of flow in the vicinity of the roughness elements. For small longitudinal spacings, vortices are formed in the grooves and the external flow skims over the tops of the roughness elements and over the enclosed vortices. This kind of geometry is called "d type" because the velocity profiles, in pipe flow, scales with the diameter. For large spacings, each element produces a wake that interacts with the following element. This is the "k type" roughness, where the height of the elements is the length scale. An

extreme case of this type is that of isolated roughness elements. Figure 5, reproduced from Young and Patterson,[20] illustrates the two types.

An attempt to consider the shape of the elements in a correlation was reported by Dirling[21] in 1973, in which he included the mean windward surface inclination. His combined, roughness density and shape parameter is:

$$\Lambda = \frac{d}{h}\left(\frac{A_f}{A_s}\right)^{-4/3}$$

where d is the average roughness element spacing and A_s is the windward surface area wetted by the flow and A_f is the frontal area of a roughness element. In 1975, Grabow and White[22] verified Dirling's correlation by showing good agreement with additional data.

Dalle Donne and Meyer[23] experimented with anulli whose inner tubes were roughened by ribs having rectangular cross-sections. They correlated their data and those of 18 previous researchers, using the roughness density parameter:

$$\lambda_h^* = \frac{p - a}{h} = \lambda_h - \frac{a}{h} .$$

For square and near square rods ($0.95 \leq h/a \leq 1.05$), their correlation gives:

$$D = \begin{cases} 5.5 - 9.3\,\lambda_h^{*-0.73} , & 1.0 \leq \lambda_h^* \leq 6.3 , \\ 5.5 - 1.04\,\lambda_h^{*0.46} , & 6.3 < \lambda_h^* \leq 160.0 . \end{cases} \qquad (12)$$

TABLE 1 contains a list of the roughness density parameters used in the past. Note that for square bars, normal to the mainstream, all the first four parameters are identical and the Dalle Donne and Meyer parameter is related to them by $\lambda_h^* = \lambda_h - 1.0$.

TABLE 1. Definitions of Roughness Density Parameters

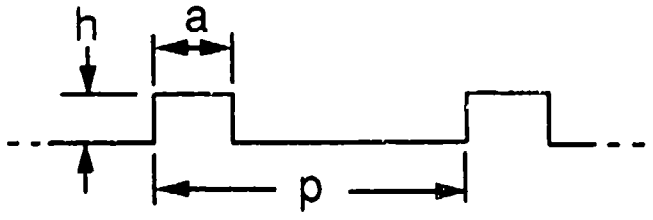

Authors	Year	Parameter	Reference
Bettermann	1965	$\lambda_h = \frac{p}{h}$	16
Dvorak	1969	$\lambda_a = \frac{p}{a}$	17
Simpson	1973	$\lambda_f = \frac{S}{S_f}$	19
Dirling	1973	$\Lambda = \frac{d}{h}\left(\frac{A_f}{A_s}\right)^{-4/3}$	21
Dalle Donne & Meyer	1976	$\lambda_h^* = \frac{p-a}{h} = \lambda_h - \frac{a}{h}$	23
Present	1988	$\Lambda_s = \frac{S}{S_f}\left(\frac{A_f}{A_s}\right)^{-1.6}$	

3. A NEW CORRELATION

Since the above mentioned correlations have been published, additional data have been reported. Furthermore, Coleman, Hodge and Taylor[24] re-evaluated Schlichting's experimental data. Their corrected values for the equivalent sand roughness are smaller, and in some cases much smaller, than those reported in Reference 14 and used in the previous correlations. Reference 24 re-evaluated three out of four of the groups of roughnesses tested by Schlichting. The corrected equivalent sand roughness for the fourth group, that of short angles, was obtained using a correlation of the available corrected versus uncorrected values. The uncertainty involved in this approximation is smaller than the scatter in the data.

The study of the available data, including the corrected data, showed that only Simpson's roughness density parameter represents the data for three-dimensional roughness configurations close to that of two-dimensional ones. Also, the inclusion of a shape factor, as proposed by Dirling, is needed in order to correlate data from roughness elements of different shapes. The new roughness density parameter is:

$$\Lambda_S = \frac{S}{S_f}\left(\frac{A_f}{A_s}\right)^{1.5} .$$

and the correlation is shown in Figure 6. The sources of the data are summarized in TABLE 2. Note that the previous correlations, plotted in Figure 6, are only valid for square or near square bars. In all these cases, the shape factor becomes unity so that the former roughness density parameters are all identical to the current one. The power of the shape factor in the current parameter has been adjusted so that it correlates Schlichting's corrected data for all four groups of roughness elements. In the case of circular rods (References 32 and 33), the streamwise area, below the point of maximum width, was accounted equal to the frontal area ($A_s/A_p = 0.5 + \pi/2.0$).

The correlation of the three-dimensional data is consistently lower than that of two-dimensional roughnesses. This difference is expected because the end effects of the finite width elements reduce their form drag relative to continuous transverse ones.

The model is biased toward data obtained on plane (rough) surfaces. For low values of the roughness density parameter, the Bettermann relationship of Equation (10), which is based on parametric wind tunnel tests, is retained. However, the large spread in the later data adds uncertainty, which only can be solved by the addition of systematic new data. For moderate and high values of the density parameter, this work proposes for two-dimensional roughness:

TABLE 2. Sources of Data Used in the Correlation

Authors	Reference	λ_h range	Comments
Schlichting	14	0.9 - 9.7	spheres
		2.6 - 15.3	spherical segments
		5.3 - 10.7	cones
		6.7 - 13.3	short angles
Bettermann	16	2.65 - 4.18	low speed wind tunnel, square bars
Dalle Donne & Meyer	23	4.08 - 61.5	annular tube, rough inner rod. Correlation includes data of several researchers and cover $2.0 \leq \lambda_h \leq 160.0$
Webb, et al	25	10.0 - 40.0	tubes
Han, et al	26	5.0 - 15.0	parallel plates, only data for transverse ribs used
Liu, et al	27	2.0 - 96.0	water tunnel
Pineau, et al	28	4.0	low speed wind tunnel, square bars
Perry & Joubert	29	4.0	
Antonia & Luxton	30	4.0	
Antonia & Wood	31	2.0	
Furuya, et al	32	2.0 - 64.0	transverse circular rods
Sherif & Gumley	33	10.0	

$$D = \begin{cases} 17.35(1.634 \log \Lambda_S - 1.0) , & 1.4 \le \Lambda_S \le 4.89 , \\ 2.2 , & 4.89 < \Lambda_S < 13.25 , \\ 9.55(1.0 - 0.686 \log \Lambda_S) , & 13.25 \le \Lambda_S \le 100.0 . \end{cases} \quad (13)$$

For dense arrangements of two-dimensional roughness elements, vortices form in the cavities and the external flow skims over the tops of the elements and the vortices. In this case, the shape factor may be different from that for sparse roughness elements. Since no additional pertinent data were found for this region, the left branch of the correlation (Equation (13)) should only be used for square, or near square, bars. The scarcity of data for three dimensional roughness at low and intermediate values of the density parameter prevents a general model for this case. A partial model for three-dimensional roughness is:

$$D = 9.7(1.0 - 0.794 \log \Lambda_S) , \; 16.0 \le \Lambda_S \le 200.0 . \quad (14)$$

4. THE EQUIVALENT SAND ROUGHNESS

Using Equation (9), the equivalent sand roughness for two-dimensional roughnesses becomes:

$$\frac{h_{es}}{h} = \begin{cases} 0.003215 \, \Lambda_S^{4.925} , & 1.4 \le \Lambda_S \le 4.89 , \\ 8.0 , & 4.89 < \Lambda_S < 13.25 , \\ 151.71 \, \Lambda_S^{-1.1379} , & 13.25 \le \Lambda_S \le 100.0 . \end{cases} \quad (15)$$

for three-dimensional roughnesses:

$$\frac{h_{es}}{h} = 160.77 \, \Lambda_S^{-1.3376} , \quad 16.0 \le \Lambda_S \le 200.0 . \quad (16)$$

These correlation equations are presented in Figure 7. The present left branch is identical to that of Bettermann and very close to that of Dirling. On the other hand, the present right branch is much higher than the previous correlations by Dvorak and Dirling. Due to the variance in the density parameters, comparison of the equivalent sand roughness is only possible for the case square bars.

5. DEPENDENCE ON MACH NUMBER

As discussed in Chapter III, the displacement of the logarithmic velocity and the gain in skin friction for sand roughness is independent of Mach number, provided the Reynolds number of the grain size is evaluated at wall conditions. Voisinet[34] reached the same conclusion for screens.

On the other hand, the only datum found for two-dimensional roughness at a supersonic speed, is that of Berg,[35] which shows an effective sand roughness that is lower than predicted by the low speed correlations. The results concerning skin friction and the intercept of the logarithmic velocity are consistent, indicating high quality data. Nevertheless, since this is a single datum, no reliable relationship between the equivalent sand roughness and Mach number can be devised. Such a relationship will have to be based on calibration of computations of the drag of roughness configurations for which data are available.

V. APPLICATION IN COMPONENT BUILD-UP METHODOLOGIES

1. COMPONENT BUILD-UP IN DRAG

The new correlation can be used for an engineering type estimate of the increment in friction drag due to surface roughness. The results of such estimates can be used with Component Build-Up (CBU) methodologies, because they add on the various contributions to the drag.

A schematic of the analysis is shown in Figure 8. Using the new correlation, the equivalent sand roughness, for a given roughness geometry is evaluated. Also, for given flight conditions and size of the flight vehicle, the smooth wall average skin-friction coefficient is estimated. Knowing these two quantities, the gain in skin friction, C_f/C_{fo} , due to roughness, is evaluated. The additional axial-force coefficient is

$$\Delta C_A = \frac{S}{S_R} \Delta C_f \ , \tag{17}$$

where $\Delta C_f = C_f - C_{fo}$.

2. LONG-ROD PROJECTILE TEST CONFIGURATIONS

The component build-up scheme and the Navier-Stokes numerical computation, to be considered in subsequent Chapters, were checked by applying them to the wind-tunnel models tested by Brandon and Von Wahlde.[36] The models were tested in the Naval Surface Weapons Center

supersonic wind tunnel and consisted of a Sears-Haack nose, a forebody, an afterbody and a fin section as shown in Figure 9. Several forebodies and afterbodies were constructed in different lengths so that the overall length could be varied between 20 and 35 calibers. The forebody sections were either smooth or grooved as shown in Figure 10. The afterbody sections were either smooth, grooved or covered with standard machine threads (30 threads/caliber). Thus a number of different kinds of roughness characteristics could be produced to simulate typical saboted projectiles. Tests were performed with and without the fins. The wind tunnel model has an abrupt 6.2% decrease in diameter at the fore- to aft-body junction.

The wind tunnel tests of the models were carried out over a Mach number range of 3.5 to 5.0. However, the majority of the tests were focused on Mach number 5.0. The Reynolds number in the wind tunnel was relatively small compared to free-flight conditions, particularly at the high Mach numbers.

3. COMPONENT BUILD-UP RESULTS

The roughness density parameter for these buttress grooves is small enough to be on the left branch of the new correlation. According to a comment in Section IV-3, the shape factor should not be used in this case. Thus, the equivalent sand roughness was estimated as if the cross-section of a groove was a square. The ratio h_{es}/h was found for two cases. The first, for $\lambda_h = p/h$ and the other for $\lambda_h' = \lambda_h + 0.5$, which takes into account the width of the cavities at their top end. An average value of the two cases is used. For the (plain) threads, the data of Fenter for v grooves was used. The estimated values are:

form	h_{es}/h
Buttress Grooves	0.52
Threads	0.55

The smooth wall skin coefficient was obtained from the NSWC Aeroprediction[37] code. For configurations with mixed roughness (buttress threads on the forebody, threads on the afterbody), separate estimates were performed for each section. The analysis followed the scheme described above and the results are shown in Figure 11 in comparison with wind-tunnel data, based on Appendix D of Reference 36. In more than half the cases, the agreement between prediction and test data is good. In the other cases, the deviations do not show a consistent trend and are of the same order of magnitude as the scatter in the data.

VI. ALGEBRAIC TURBULENCE MODELS FOR NUMERICAL CODES

In Sections IV and V, the concept of equivalent sand roughness was explored in some detail. The added drag was estimated for a given configuration using the component build-up technique. Another approach, that is potentially more general, is to modify the algebraic turbulence models used in existing numerical Navier-Stokes solvers to account for surface roughness. The distributed roughness approach does not consider the details of the roughness elements, so it is not simply a matter of changing local boundary conditions at the surface. The effect of the roughness is incorporated by changing the equations which define the relationship between the turbulent eddy viscosity and the local flow variables. Since most codes use some form of a two-layer mixing-length method for computing the eddy viscosity, the effect of roughness is to modify the mixing-length formulation. Several researchers have studied this problem and the results of their analyses are discussed in this section followed by details of the incorporation of one of them into a parabolized Navier-Stokes code and its application to the Brandon experiment.

1. VAN DRIEST MODEL

The first mixing-length model that considers wall roughness was developed by Van Driest[38] (the superscript + indicates wall units):

$$l^+ = \kappa y^+\left[1 - \exp\left(\frac{-y^+}{26}\right) + \exp\left(\frac{-60y^+}{26h_s^+}\right)\right], h_s^+ \le 60 . \qquad (18)$$

The value $h_s^+ = 60$ marks the beginning of the region of fully rough flow. For this value the wall damping is eliminated and the mixing length becomes:

$$l^+ = \kappa y^+ \quad \text{at} \quad h_s^+ = 60 .$$

According to this model, l vanishes at the wall in the entire range of applicability, as illustrated in Figure 12. The initial slopes of the l^+ vs y^+ curves are equal to κ, except for the case of a smooth surface, where the initial slope vanishes. To apply this method to larger roughness ($h_{es}^+ > 60$) requires additional empirical information concerning the displacement in y of the effective wall.

2. HEALZER MODEL

Several researchers proposed extensions of the mixing-length model into the region of fully rough boundary layer, by allowing the mixing length to exceed κy^+ and become non zero at the wall. The one by Healzer,[39] et al was considered for application because it was successfully used

by Lin and Bywater.[40] It has been selected for inclusion in the PNS code because it is compatible with the Baldwin-Lomax turbulence model already in the code, it is directly adopted to compressible flow, and it is not limited in roughness height which can be considered.

$$l^+ = \begin{cases} \kappa y^+\left[1 - \exp\left(\frac{y^+}{A_R}\right)\right] \quad , \quad 7 < h_s^+ \le 55 \ , \\ \text{with } A_R = 12.615\left(4.007 - \ln h_s^+\right) \quad ; \\ \left[(\kappa y^+)^2 + (\Delta l_o)^2\right]^{1/2} \quad , \quad h_s^+ > 55 \quad . \\ \text{with } \Delta l_s^+ = \left[\left(\frac{h_s^+ - 46}{39}\right)^2 - 0.05325\right]^{1/2} \quad . \end{cases} \tag{19}$$

For intermediate roughness, the mixing length and its initial slope vanish at the wall. For a fully rough wall, l^+ equals Δl_o^+ at the wall. The wall value increases, as h_s^+ increases, as shown in Figure 13.

3. HAN MODEL

More recently, Han[41] developed a new formulation for the mixing length for smooth surfaces and extended it to rough ones. His approach is different from all previous ones in relating the mixing length to the velocity, rather than to the distance from the wall. Four models were studied by Han, the preferred one being

$$l^+ = R\frac{\kappa}{E}\left[\exp(\kappa U^+) - \exp(-\kappa U^+)\right] \ , \tag{20}$$

with E = 9.025 and R, the roughness amplification factor, a function of the shape of the roughness and of h^+. For sand grain roughness:

$$R = 0.3036\, h_s^+ \quad , \quad h_s^+ > 100 \ . \tag{21}$$

For $h_s^+ < 100$, Han provides tabulated values of R. Study of the data showed that the above expression can be used down to $h_s^+ = 50$ with a very small inaccuracy. The following model is proposed

$$R = \begin{cases} 0.3036\, h_s^+ \quad , \quad h_s^+ > 50 \ , \\ 0.3036\, h_s^+ - 0.043(50 - h^+) \quad , \quad 20 < h_s^+ < 50 \ . \end{cases} \tag{22}$$

It should be noted that the Han model is based on the incompressible logarithmic velocity profile and as a consequence it is not apparent how this formulation can be extended to high speed compressible flows.

4. THE OUTER LAYER

Clauser[8] reached a conclusion that the turbulence level and the Reynolds stresses in the outer layer are not affected by wall roughness. Since then, most researchers have accepted this finding. Thus in the following, the Baldwin-Lomax outer-flow computational procedure is used.

VII. APPLICATION TO PARABOLIZED NAVIER-STOKES CODE

1. PARABOLIZED NAVIER-STOKES CODE

The Parabolized Navier-Stokes equations (PNS) have been solved using a technique developed by Schiff and Steger.[42] These equations, in strong conservation form, and simplified using the thin shear layer approximation can be written in generalized coordinates as follows:

$$\frac{\partial \hat{E}_S}{\partial \xi} + \frac{\partial \hat{F}}{\partial \eta} + \frac{\partial \hat{G}}{\partial \zeta} = \frac{1}{\hat{R}e} \frac{\partial \hat{S}}{\partial \zeta} \tag{23}$$

where ξ, η, ζ are the generalized coordinate variables.

$\xi = \xi(x)$, is the longitudinal (marching) coordinate
$\eta = \eta(x,y,z)$, circumferential coordinate
$\zeta = \zeta(x,y,z)$, near normal coordinate.

The inviscid flux vectors $\hat{E}_S$, $\hat{F}$, and $\hat{G}$ and the viscous matrix terms, $\hat{S}$, are functions of the dependent variables, $\hat{q}$:

$$\hat{q} = J^{-1} \begin{pmatrix} \rho \\ \rho u \\ \rho v \\ \rho w \\ e \end{pmatrix} \tag{24}$$

where ρ is the density, ρu, ρv, and ρw are the mass fluxes in the three coordinate directions and e is the total energy per unit volume The local pressure is determined by using the relation:

$$P = (\gamma - 1)[e - 0.5\rho(u^2 + v^2 + w^2)] \tag{25}$$

where γ, is the ratio of specific heats. The parabolization of the equations is accomplished in the $\hat{E}_S$ flux vector by ensuring that the static pressure is maintained constant across the subsonic layer near the wall. Thus, in supersonic free-stream flows, these equations can be solved by marching in the longitudinal direction.

An initial plane of data is required to begin the marching and this is obtained from the conical starting procedure. The starting procedure consists of marching one step downstream and updating the previous step by extrapolating back using a conical flow assumption. This procedure is repeated until a converged solution is obtained in which the change in density between successive iterations is less than 10^{-5} times the free-stream value.

The numerical algorithm is formulated using an approximately factored, implicit, finite difference scheme developed by Beam and Warming.[43] Fitting of the outer bow shock wave has been performed in these calculations consistent with the implicit boundary method formulated by Rai and Chaussee.[44]

2. IMPLEMENTATION OF THE TURBULENCE MODEL

The PNS code employs the Baldwin-Lomax[45] smooth wall turbulence model and the viscous flow is assumed turbulent from the starting solution. The Baldwin-Lomax model is a two layer model in which the inner layer eddy viscosity is defined by:

$$\mu_t^i = \rho l^2 |\omega| \tag{26}$$

where $l = ky\left[1 - \exp\left(-\frac{y^+}{A^+}\right)\right]$ and $|\omega|$ = magnitude of the vorticity

and for attached flow, the viscosity in the outer layer is given by:

$$\mu_t^o = KC_{cp}\rho y_m F(y_m)\Gamma \tag{27}$$

where $F(y) = y|\omega|\left[1 - \exp\left(-\frac{y^+}{A^+}\right)\right]$

and $F(y_m)$ = maximum of $F(y)$ and y_m is the normal distance to the maximum in $F(y)$.

$K = 0.0168$

$C_{cp} = 1.6$

$$\Gamma = \left[1 + 5.5\left(\frac{C_{kleb}y}{y_m}\right)^6\right]^{-1} = \text{(Klebanoff intermittency factor)}$$

$C_{kleb} = 0.3.$

The inner viscosity is used at each step normal to the wall until it exceeds the outer viscosity where upon the outer value is used.

The original coding of the Baldwin-Lomax technique evaluated the eddy viscosity between grid points and interpolated to form the viscosity at the grid points for the subsequent calculations. This unnecessary step has been eliminated by Weinacht[46] and it is his version that has been used here.

The Healzer, et al.[39] model, as well as the other models discussed in Section VI, is assumed to only affect the inner layer mixing length and that the outer layer formulation remains unchanged. When the roughness model was implemented, the solution at the roughness oscillated strongly and in many cases diverged. It was observed that in a distributed roughness method, the roughness is viewed as a change in the wall boundary conditions whereas the Healzer model not only affects the wall conditions but actually changes the eddy viscosity formulation across the inner boundary layer. Physically, diffusion of wall conditions should be limited to a zone of influence, at least roughly corresponding to the propagation of a Mach wave across the layer. A convenient implementation of this idea involves freezing the eddy viscosity at its value at the start of the roughness zone above a Mach wave originating at the start of the roughness. Below the Mach wave, the eddy viscosity is calculated by the Healzer model but multiplied by a transition factor which smoothly connects the roughness eddy viscosity with the viscosity above the wave. A further simplification is made by calculating the Mach line location based on the free-stream Mach wave direction and ignoring the actual Mach number distribution including the subsonic layer. Thus the eddy viscosity distribution is calculated over the roughness section by:

$$\mu_t = \mu_t^s + (\mu_t^r - \mu_t^s)\, G \tag{28}$$

where: $\mu_t^s = \mu_t^s(y)$

= the smooth wall eddy viscosity at the start of the roughness

μ_t^r = rough wall eddy viscosity

G = transition factor

The factor, G, is chosen to have the following form,

$$G = \begin{cases} 1 & \dfrac{y_{mw} - y}{y_m} > 1 \\ 1 - \exp\left[-\left(\dfrac{y_{mw} - y}{y_m}\right)^2\right] & 0 < \dfrac{y_{mw} - y}{y_m} \le 1 \\ 0 & \dfrac{y_{mw} - y}{y_m} < 0 \end{cases}$$

$$y_{mw} = (x - x_{ri}) \tan\left[\arcsin\left(\frac{1}{M_\infty}\right)\right]$$

= location of Mach wave

x_{ri} = longitudinal start of the roughness area

y = distance normal from the wall

y_m = Baldwin-Lomax normal distance to maximum in moment of vorticity.

Note that when y_{mw} is significantly larger than the viscous layer, the eddy viscosity is computed entirely based on the rough wall model. The form and extent of the transition region is quite arbitrary except that eddy viscosity should smoothly change from the smooth wall to rough wall value over as small of a region of the rough surface as is needed for numerical stability.

The downstream transition from the rough wall to the smooth wall potentially presents a similar problem of the discontinuous change in the equations used to compute the mixing length. A transition may be expected where the smooth wall turbulence diffuses out from the change in the wall boundary condition. In the present case, it was not necessary to introduce a transition process, although the skin friction decreased to very low values behind the roughness and could possibly go to zero or become negative for larger roughnesses. The PNS code would not be valid under these conditions, nor would the Healzer turbulence model be applicable.

3. APPLICATION TO A LONG-ROD PROJECTILE

As previously noted, the computations with the roughness model have been applied to the flow conditions and configuration tested by Brandon and Von Wahlde.[36] The model configuration is shown in Figures 9 and 10.

The blunt tip of the Sears-Haack nose (0.035 caliber) is replaced by a 14.972 degree conical tip which increased the total length to 20.757 calibers for the smallest L/D model. No forces are calculated in the conical tip and thus the axial forces are somewhat less than would be obtained in the experiment. The origin of the computational coordinate system is at the virtual origin of the conically extended nose. The change in diameter between the fore- and aft-body is implemented in the computations as a conical section, of about one caliber, in order to reduce numerical oscillations due to the change in geometry. The PNS computations were made corresponding to a Mach number of 5.0, Reynolds number of 18.6×10^6 per meter and a nominal wall temperature of 300 K.

The geometry of the groove roughness elements are shown in Figure 10. The test configuration computed here consists of groove roughness elements extending over the entire fore- and aft-body and just on the fore-body. The groove depth is 0.0535 calibers and its pitch is 0.1334 calibers. The front face of each element is inclined at approximately a 45 degree angle. As has been previously pointed out, this roughness is such that the roughness density correlation is not valid and the equivalent sand roughness height has been estimated in Section V to be 0.0278 calibers. However, the computations have been performed over a range of values of equivalent roughness height.

4. PNS RESULTS

Figure 14 shows the skin friction coefficient distribution for the case of an equivalent roughness height of 0.0278 calibers. The solid line is the smooth body case and the dashed line is with groove roughness over the fore- and aft-body. There is considerable oscillation at each change in the body shape which is frequently observed in PNS skin friction results. Skin friction is an extremely sensitive result because it mainly depends on the derivative of the velocity profile. Increased numerical damping could possibly reduce this to some extent but potentially at some loss in accuracy.

At the leading edge of the roughness there is a very sharp peak in the wall friction but the effect of this on the properties of the boundary layer is limited by the outward diffusion as previously discussed. Downstream of the transient, the friction coefficient becomes nearly a constant factor of 1.5 higher than the smooth wall case. The abrupt transition from rough to smooth downstream of the aft body induces strong oscillations in the friction but these damp out after about four calibers. The friction considerably under-shoots the return to the smooth case

and slowly approaches it from below. The conical transition section between the two different diameter cylinders shows some relatively strong effects of the changing local flow on the roughness computation.

Figure 15 shows the effect of the roughness on the surface pressure distribution is very weak under these conditions. There is a slight increase in pressure near the start of the roughness and a slight decrease downstream of the roughness. These changes reflect the increased rate of growth of the boundary layer thicknesses over the rough portion of the body. Note that the oscillations in the solutions are much weaker in the pressure as compared to those in the friction.

Figure 16 illustrates the effect on the velocity profiles. The most distorted profile occurs at the most downstream point. Except for that one profile, the rest show the expected growth in the boundary layer thickness.

The total forebody drag results are shown, in Figure 17, as a function of equivalent roughness height. Two cases are shown, the first has roughness over both the fore- and aft-body cylinders. The second case is for the situation with roughness only on the fore-body. The smooth body calculation is in good agreement with the experiment (it is four percent lower because of the omitted nose blunting). There is a break in both curves which occurs at the point where the Healzer model changes from h_s^+ less than, to greater than 55.0. The horizontal dotted lines show the measured drag for the two cases. The equivalent sand roughness is 0.075 inches for the case where both surfaces are roughened and 0.05 inches for the rough fore-body. Both of these values are significantly different than the predicted equivalent roughness height. However, the experimental uncertainty in the drag due to roughness is potentially quite large and this could have a significant effect on the equivalent sand roughness height determined from Figure 17.

XI. CONCLUSIONS

Based on a review of previous correlations of the effect of roughness on the turbulent boundary layer, a new roughness density parameter is proposed. It is a product of reference surface to total frontal area ratio and a shape factor which takes into account the average inclination of the windward surface of the roughness elements. The new parameter is used to correlate the displacement of the logarithmic wall profile for two-dimensional and three-dimensional roughness elements. The equivalent sand roughness, based on the new correlation, is identical to, or in good agreement with, previous ones, for small values of the roughness parameter. However, for large values of this parameter, the differences are considerable.

For dense two-dimensional roughness, the ratio of the size of the equivalent roughness to height of the actual element, strongly depends on the roughness density parameter. However, because of the variability of the limited available data, the correlation results for values of the roughness parameter less than five are restricted to rectangular elements.

Additional data are needed in order to extend and further substantiate the correlation. For the two-dimensional case, data for chamfered elements are desired, and for three-dimensional roughness, elements of various aspects ratios (spanwise dimension to height ratio) in different densities and arrangements. The additional data are required, mainly, in order to extend the correlation to small and intermediate values of the roughness density parameter. In addition, compressibility effects at supersonic Mach numbers are still poorly understood.

A modified form of Bettermann's correlation has been used in an engineering type, component build-up, analysis for the estimation of the additional axial-force due to grooves and threads.

A turbulence model, based on that of Healzer, et. al. and the equivalent sand roughness correlation has been incorporated in the Schiff and Steger Parabolized Navier-Stokes code. This code has been applied to the long-rod, wind tunnel model of Brandon and Von Wahlde. It is observed that the Healzer model has to be modified to include a transition zone when going from a rough to a smooth surface and vice verse. This is required to obtain stable numerical solutions and to account for the propagation of information across the viscous layer at high speeds. The propagation is approximated by restricting the effect of the changing wall conditions to a region below a Mach wave originating at the change in wall conditions. The wave has been estimated using the free-stream Mach number.

The modified PNS code has been applied to the wind tunnel tests of Brandon and Von Whalde. When the predicted equivalent roughness height of 0.0278 calibers was used in the code, the skin friction coefficient is increased on the roughened surface 48% over the smooth wall case. This is consistent with the component build up method. Additionally, the PNS results predict the skin friction to be below (up to 20%) the smooth wall value on the surfaces downstream of the roughness. The component build-up technique did not account for this reduction.

The total drag computed from the modified PNS code using the predicted equivalent roughness height is significantly lower than the drag measured in the wind tunnel. A larger equivalent roughness height corresponding to the actual roughness gave better results.

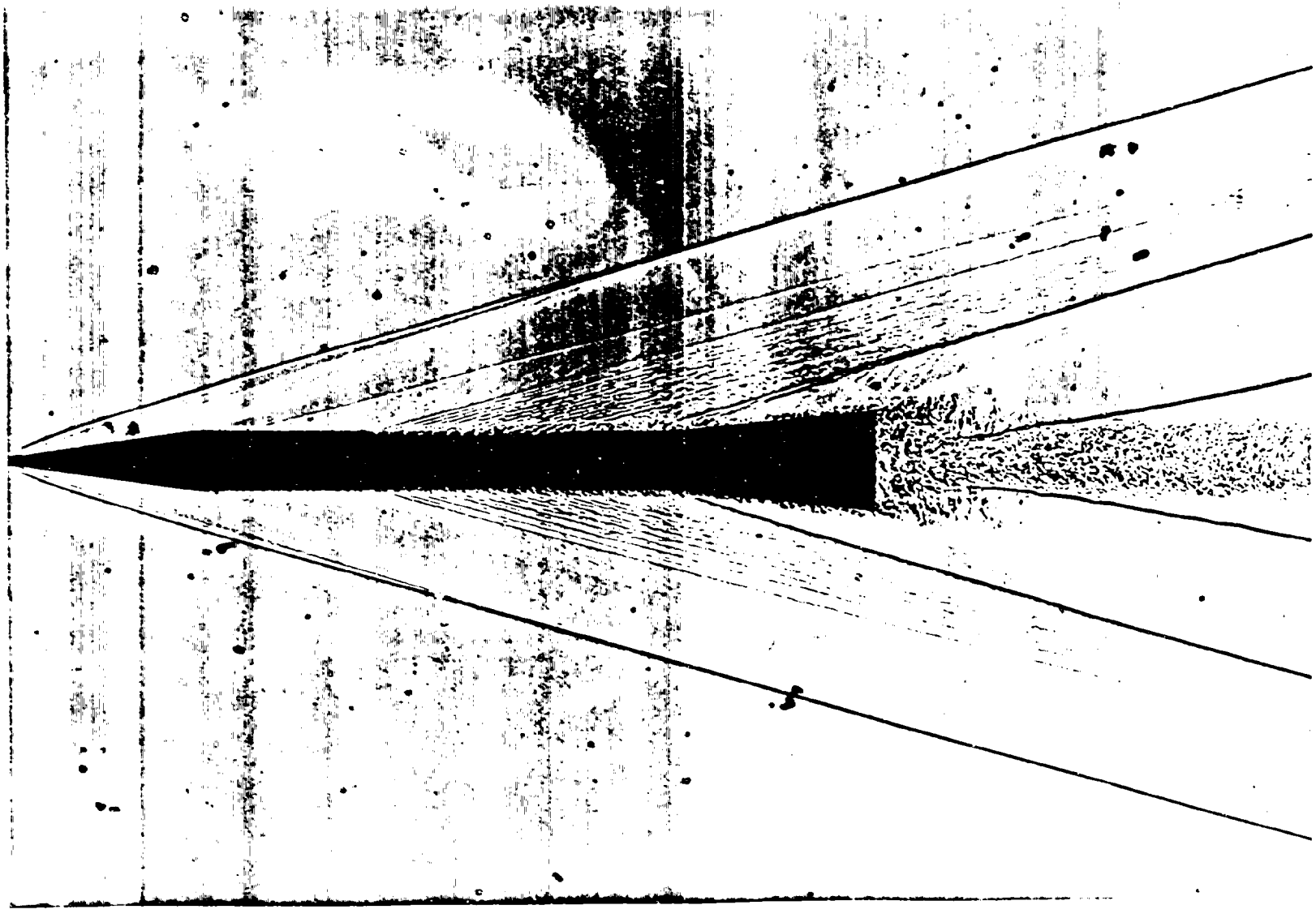

Figure 1. Spark shadowgraph of a high velocity penetrator in flight.

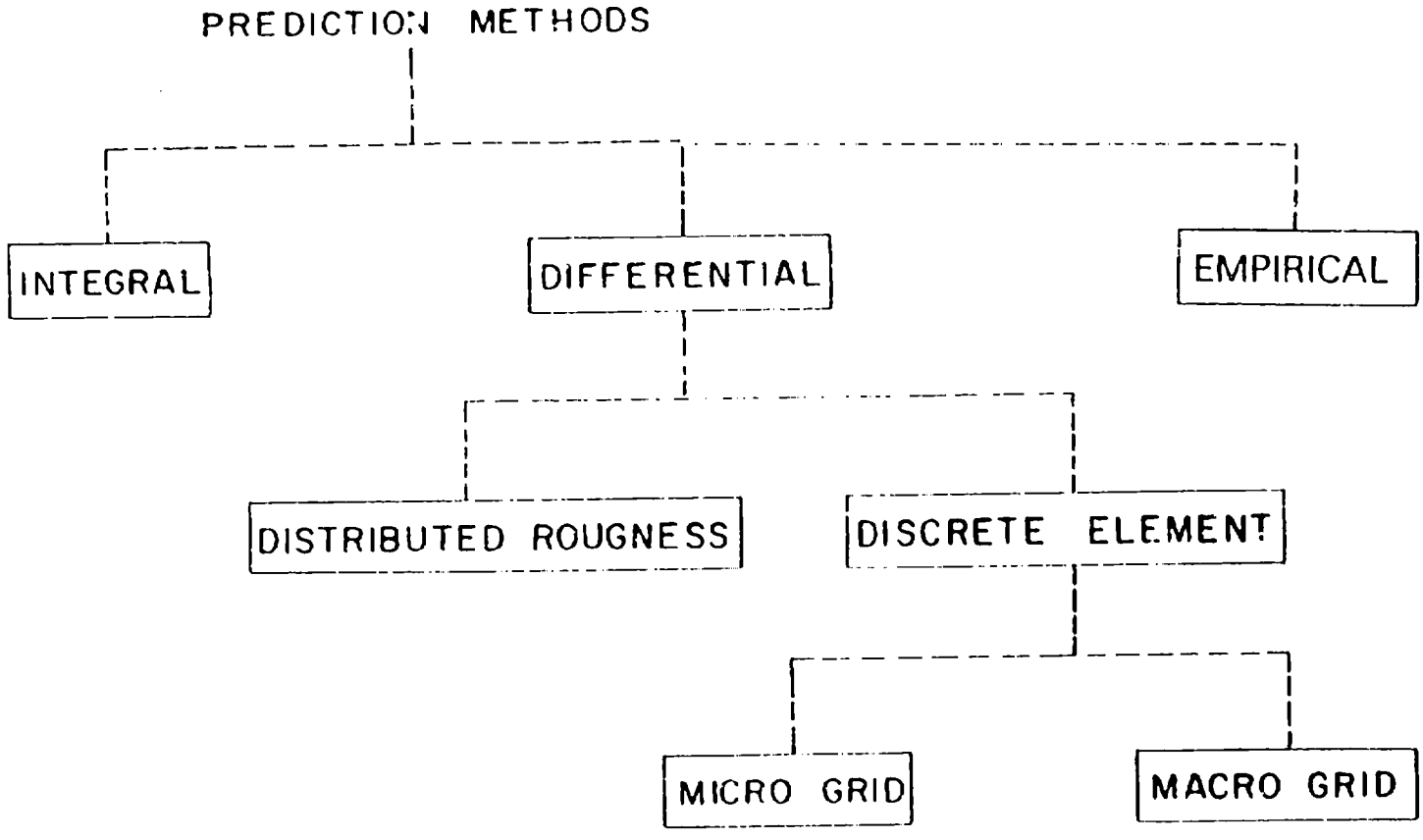

Figure 2. Classification of predictive methods for turbulent boundary-layer over rough surfaces.

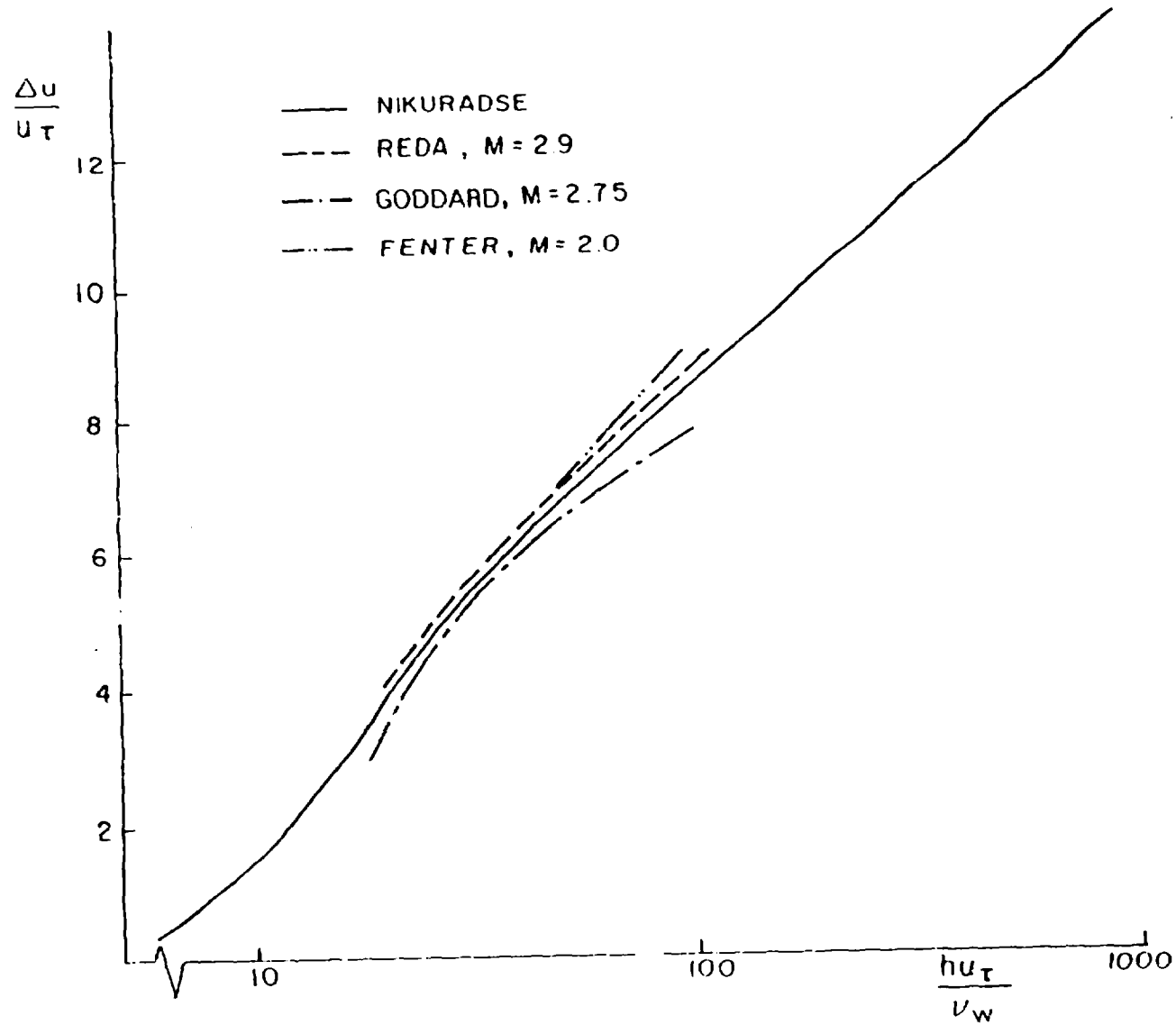

Figure 3. The effect of sand roughness on the Law of the Wall intercept.

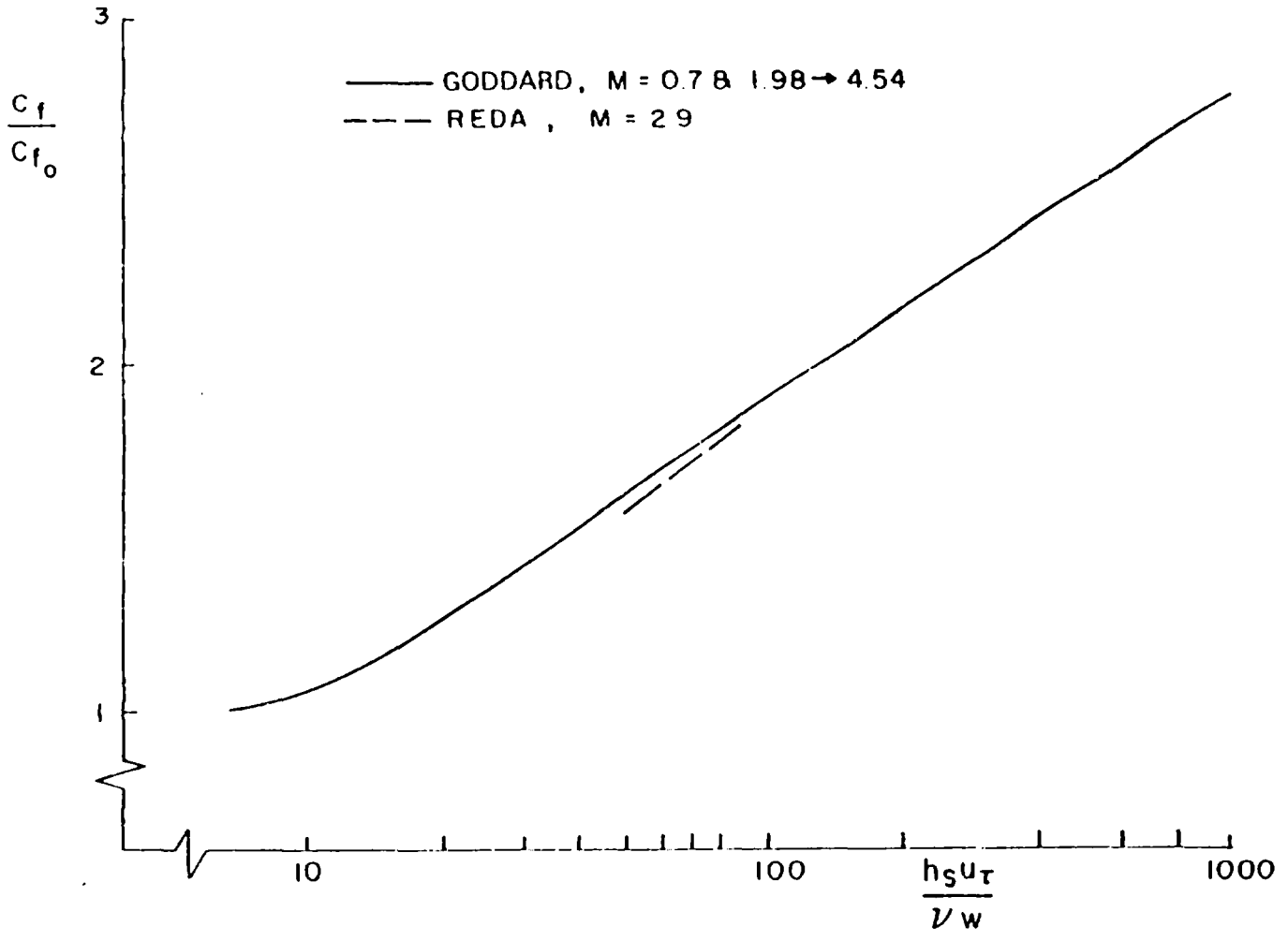

Figure 4. Ratio of rough wall to smooth wall skin friction coefficient for sand roughness.

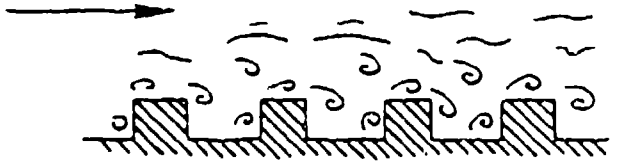

'k' TYPE ROUGHNESS

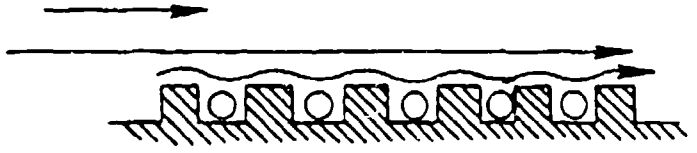

'd' TYPE ROUGHNESS

Figure 5. Illustration of 'k' and 'd' roughnesses (after Reference 20).

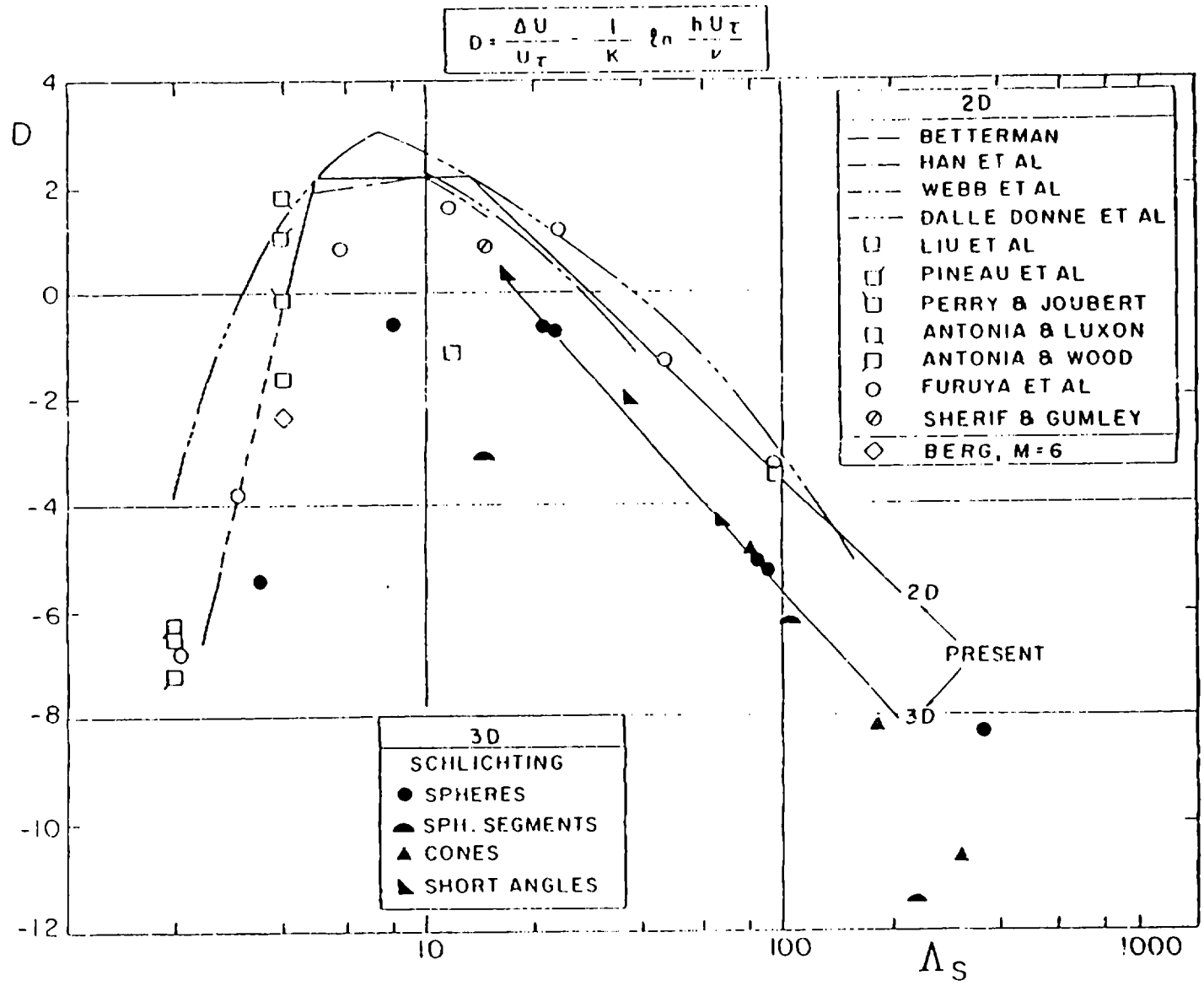

Figure 6. Correlation of the effect of roughness density on the Law of the Wall Intercept.

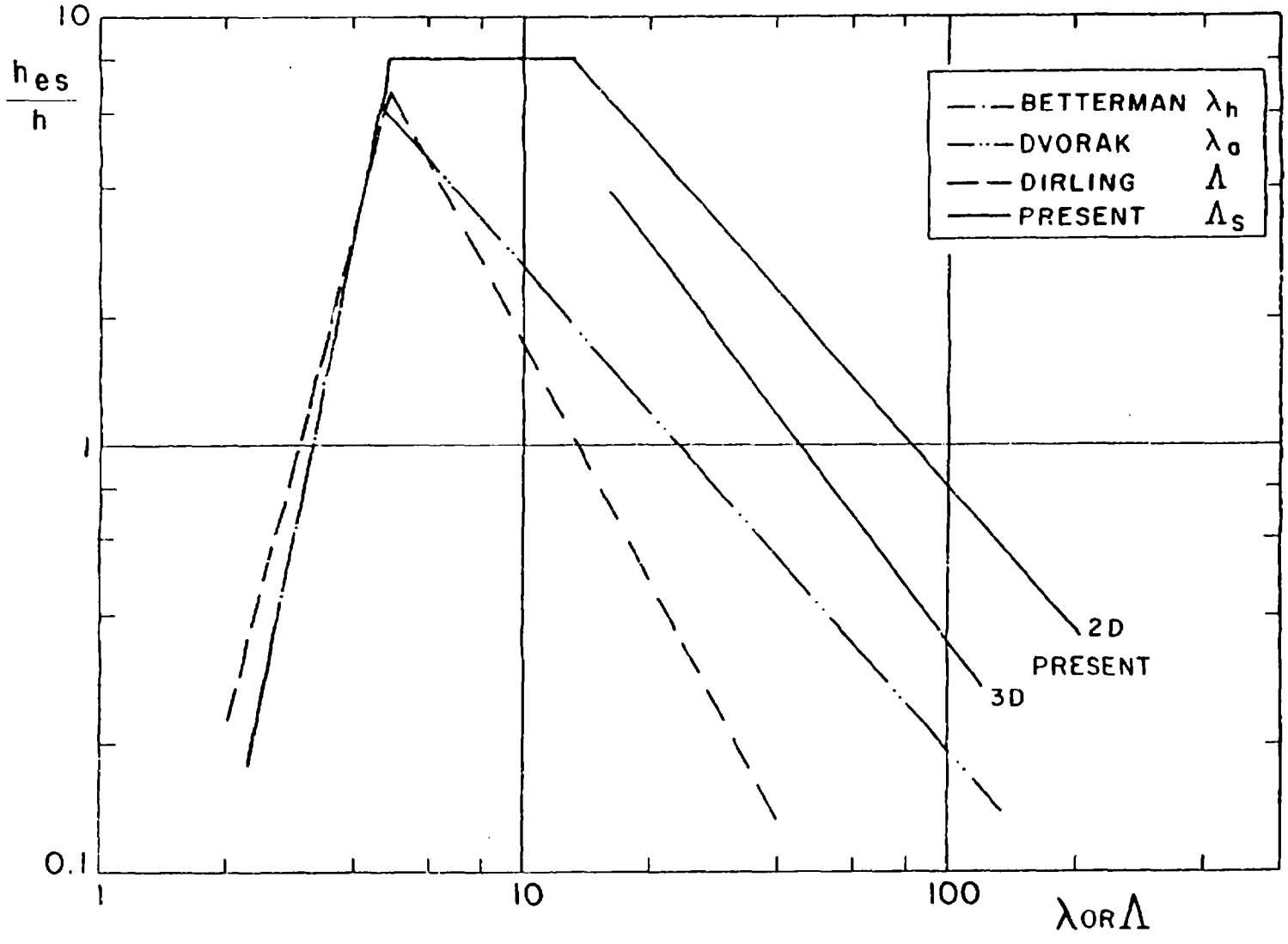

Figure 7. Correlation of the effect of roughness density on equivalent sand roughness.

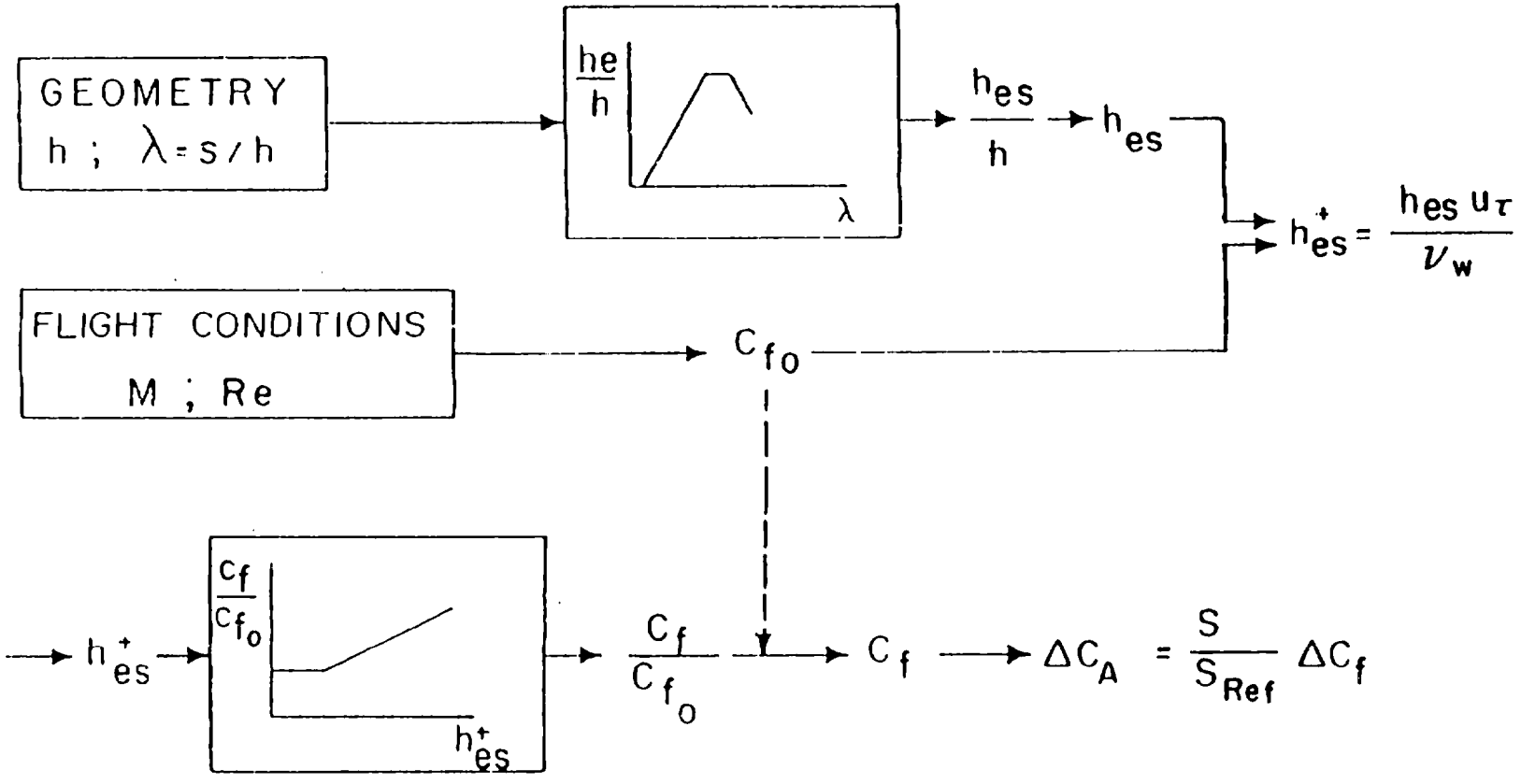

Figure 8. Scheme of estimation of the axial-force due to roughness (component build-up analysis).

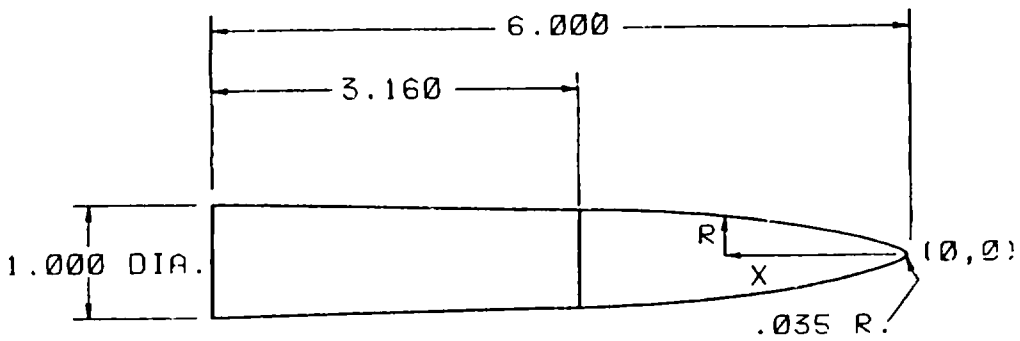

$$R = .432 * (1. - (1. - 2. * X/5.995)^2)^{.75}$$

$$0.0 \leq X \leq 2.839$$

(ALL DIMENSIONS IN CALIBERS)

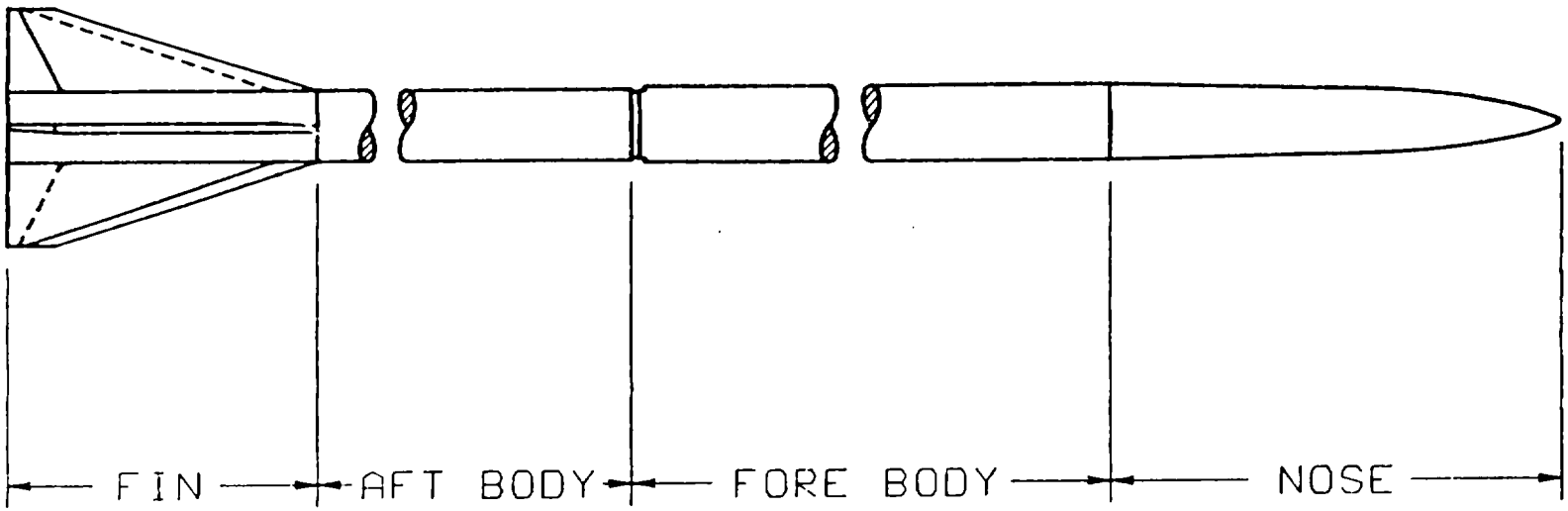

Figure 9. Brandon and Von Whalde wind tunnel model assembly.

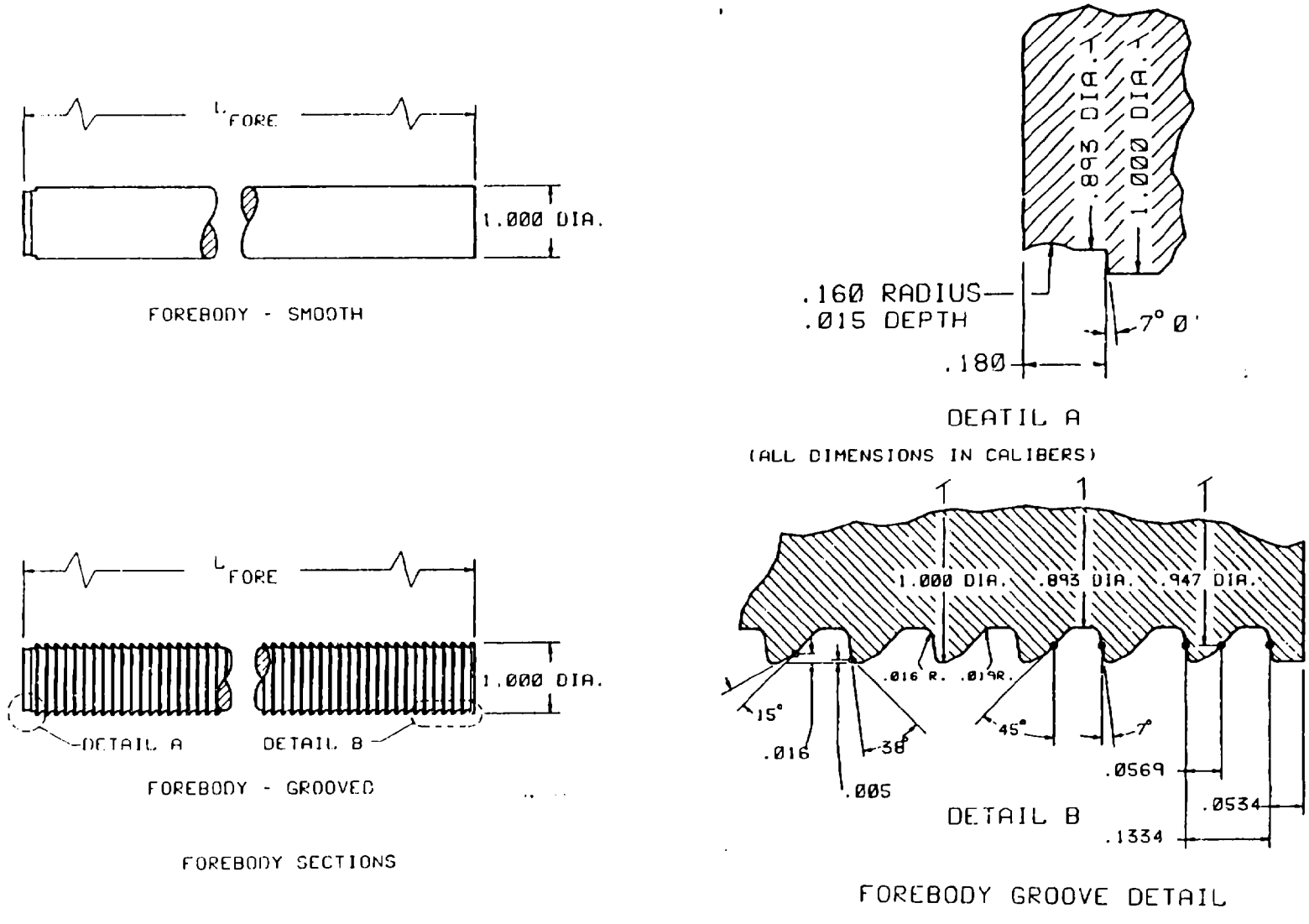

Figure 10. Forebody section and grooves detail of the Brandon and Von Whalde wind tunnel model.

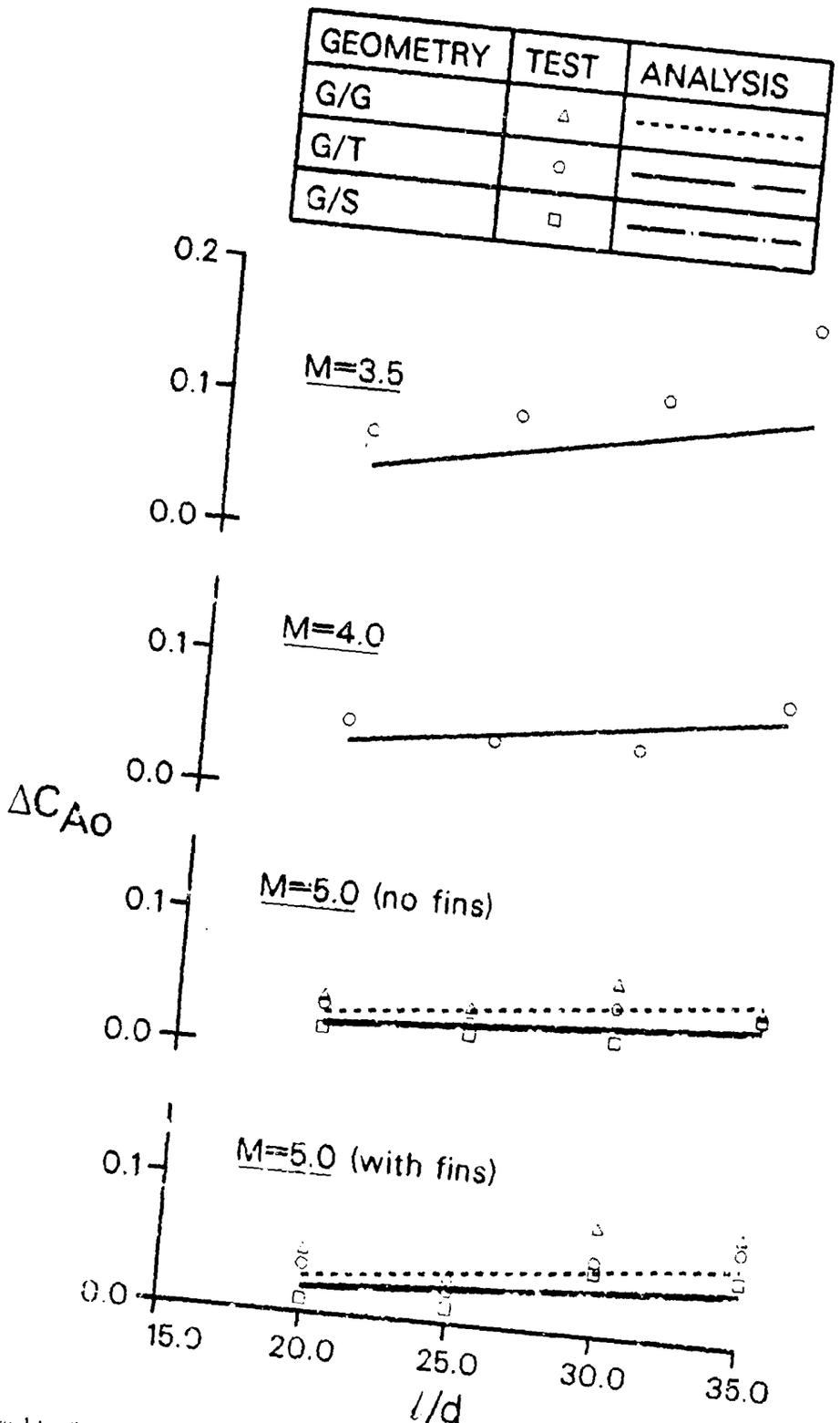

Figure 11. Comparison between predicted and experimentally obtained axial-force due to grooves and threads.

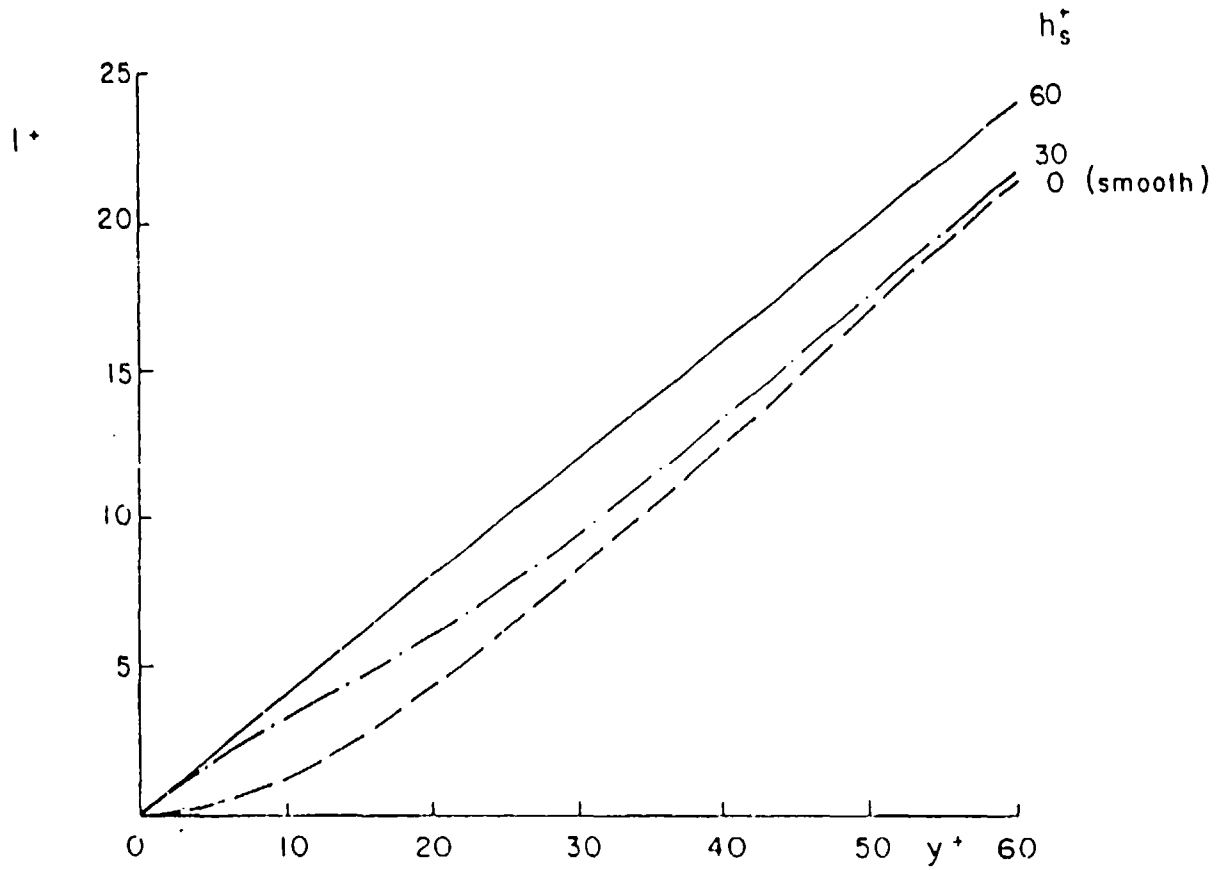

Figure 12. Nondimensional mixing length based on the Van Driest model.

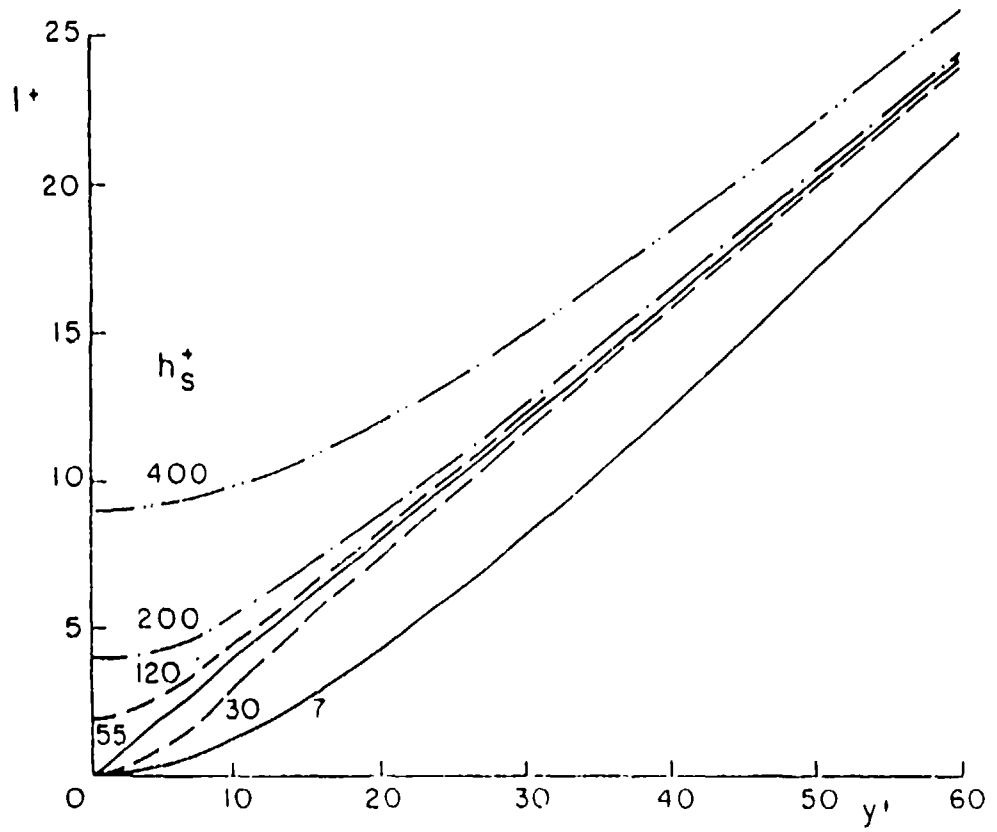

Figure 13. Nondimensional mixing length based on the Healzer, et al model.

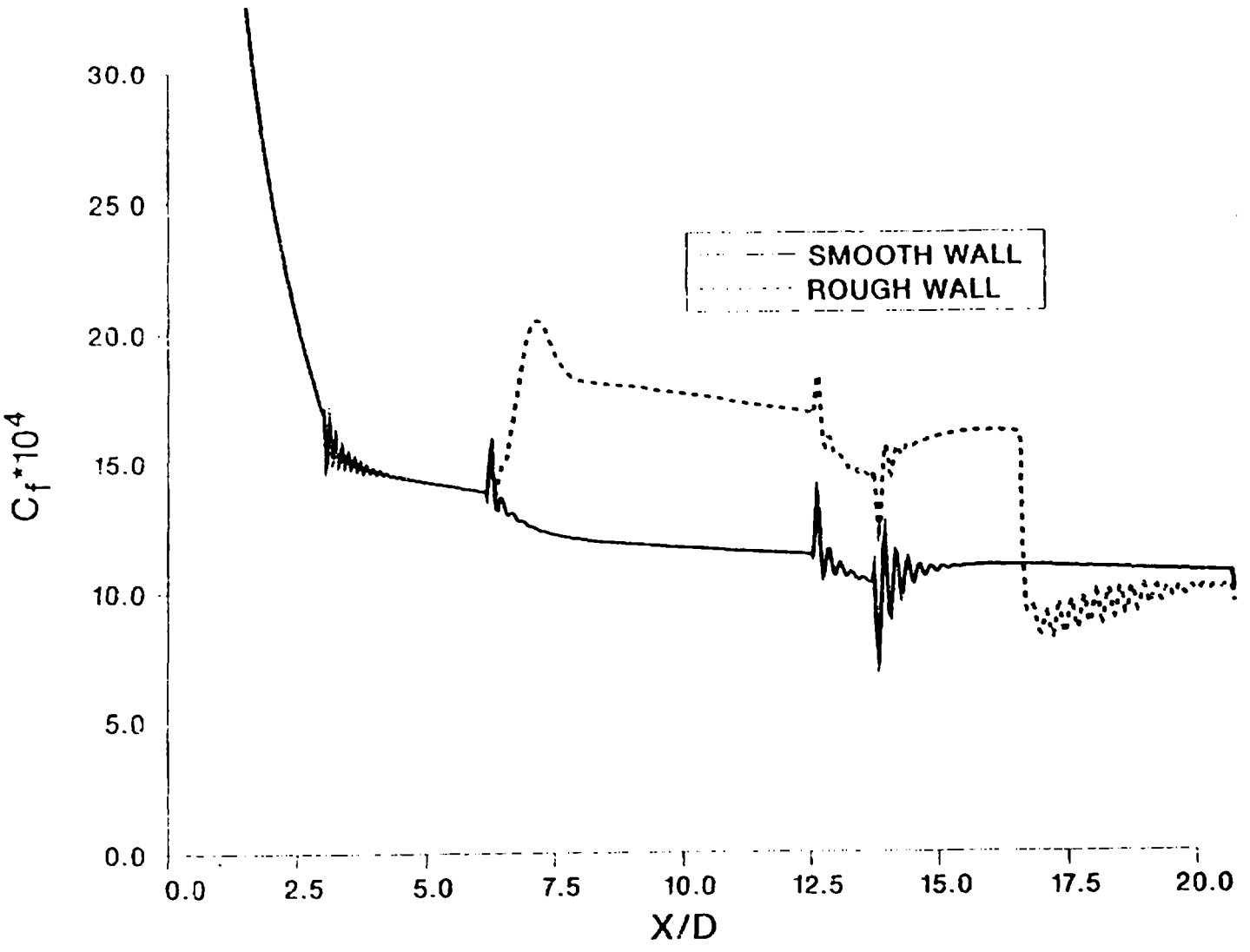

Figure 14. PNS code prediction of the skin friction for the Brandon and Von Whalde wind tunnel model.

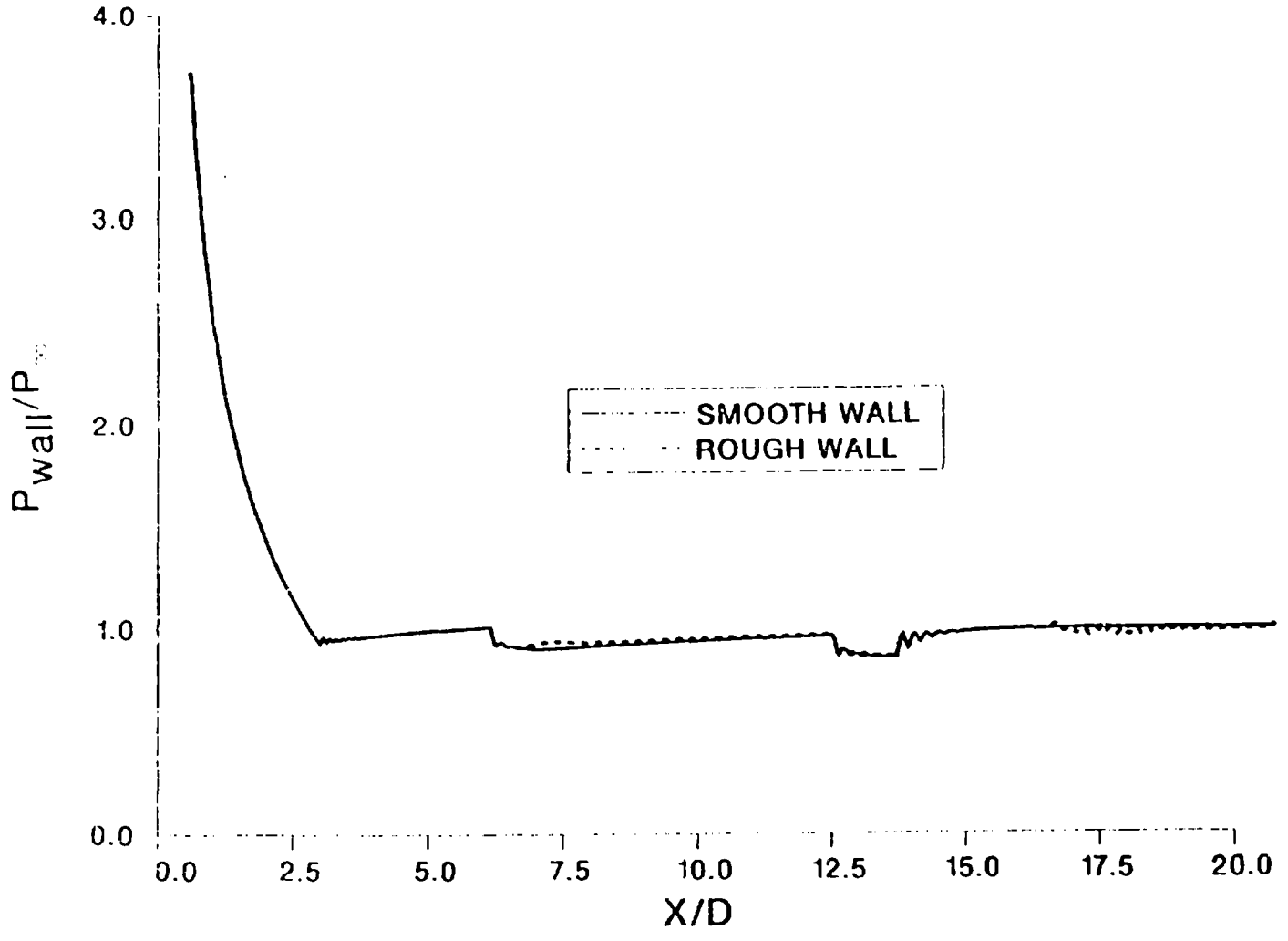

Figure 15. PNS code prediction of the pressure distribution for the Brandon, et al wind tunnel model.

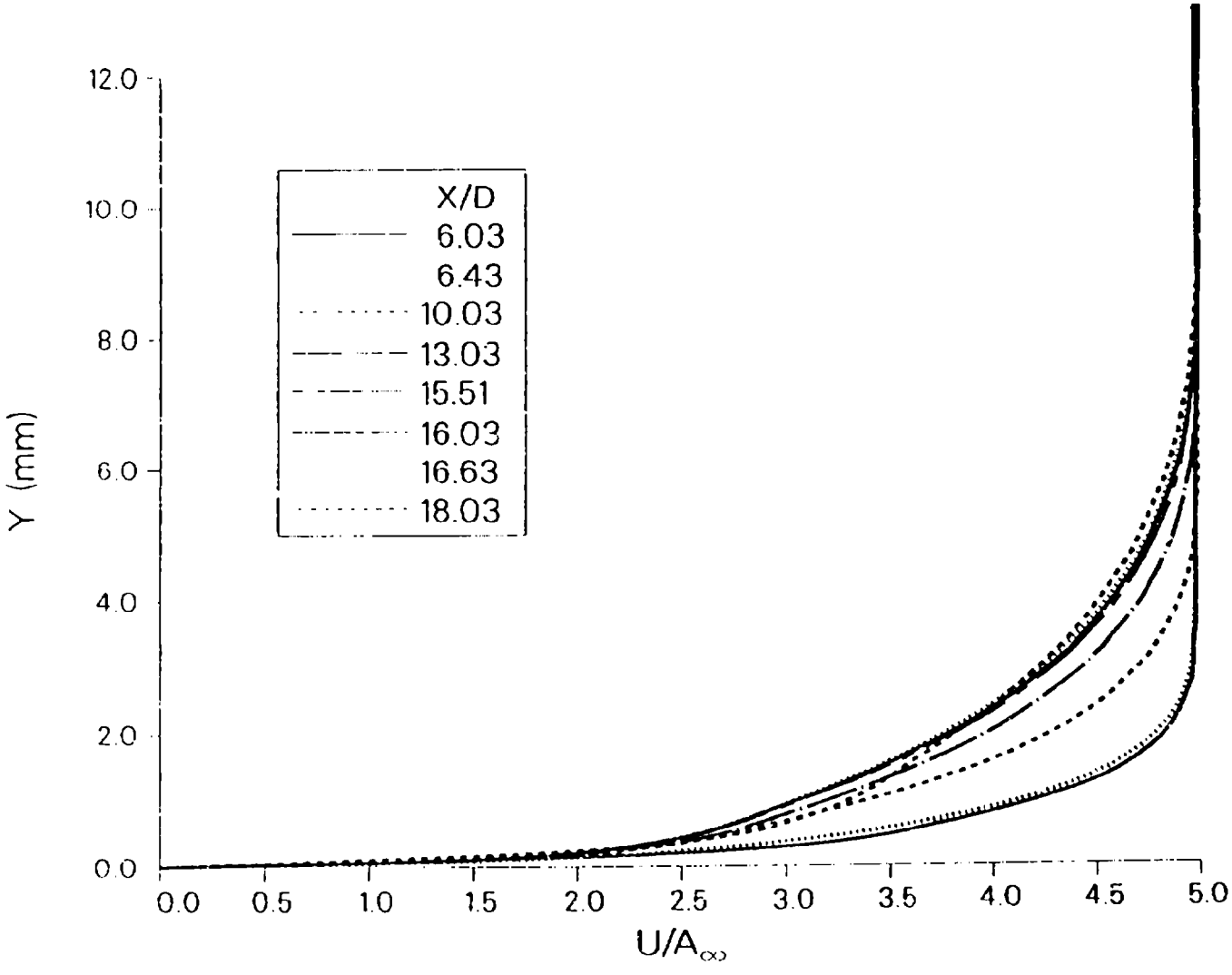

Figure 16. Representative velocity profiles over the rough surface.

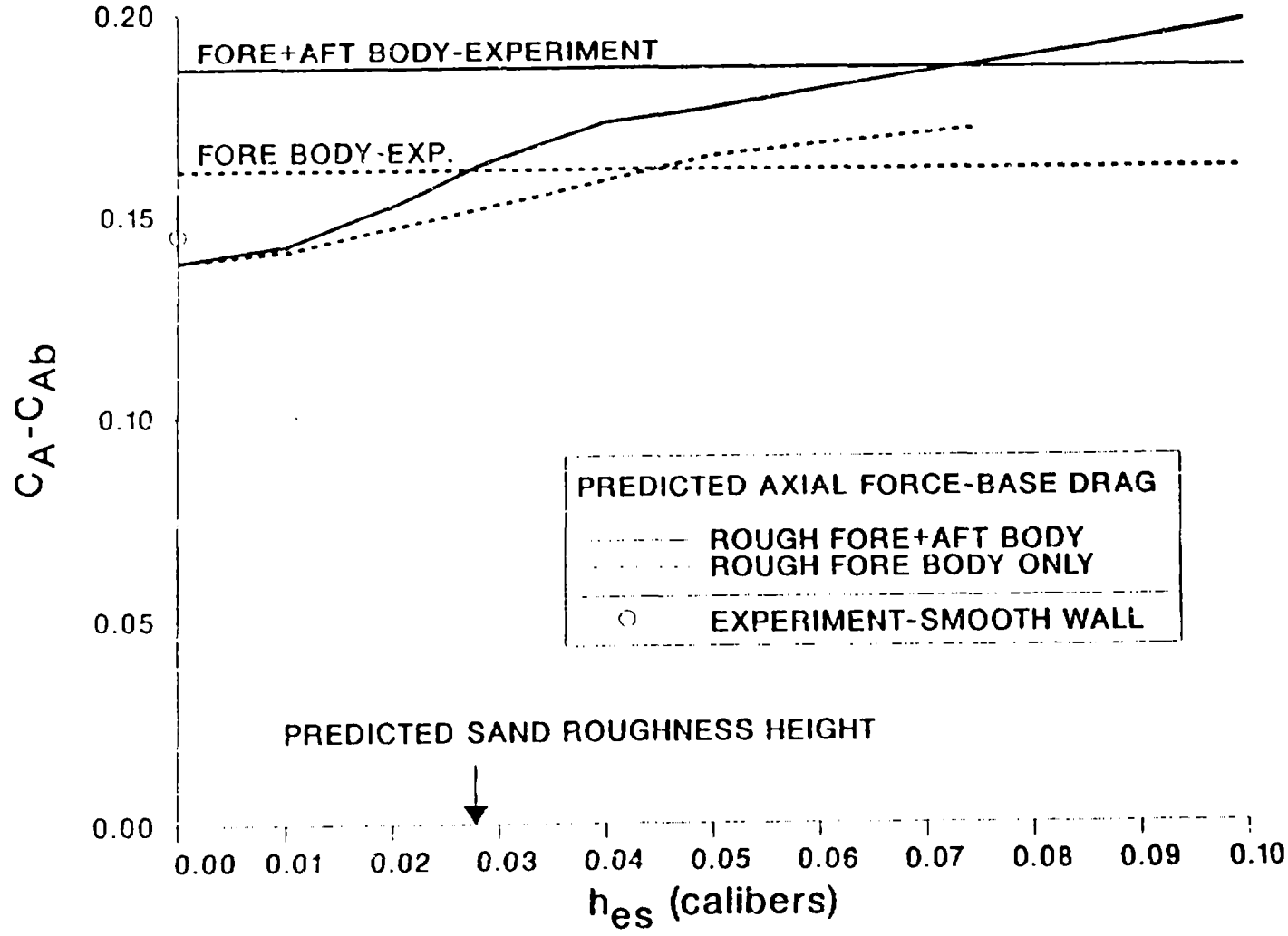

Figure 17. Forebody axial-force as a function of equivalent roughness height.

REFERENCES

1. Mikhail, A.G., "Data Correlation and Prediction of Surface Grooves Drag for Kinetic Energy Projectiles," AIAA Paper No. 88-2541, Proceedings of the 6th Applied Aerodynamics Conference, June 1988.

2. Sahu, J. and Danberg, J.E., "A Combined Computational and Experimental Study of Supersonic Flow Over a Protuberance," AIAA Paper No. 87-2291, Proceedings of the Atmospheric Flight Mechanics Conference, Monterey, CA, August 1987.

3. Baysal, O. and Stallings, R.L., "Computational and Experimental Investigation of Cavity Flowfields," AIAA Paper No. 87-0114, Proceedings of the 25th Aerospace Sciences Meeting, Reno, NV, January 1987.

4. Venkataphaty, E., Lombard, C.K. and Nagaraj, N., "Numerical Simulation of Compressible Flow Around Complex Two-Dimensional Cavities," AIAA Paper No. 87-0116, Proceedings of the 25th Aerospace sciences Meeting, Reno, NV, January 1987.

5. Hodge, B.K. and Adams, J.C., "The Calculation of Compressible Transitional, Turbulent, and Relaminarizational Boundary Layers Over Smooth and Rough Surfaces Using an Extended Mixing-Length Hypothesis," AEDC-TR-77-96, Arnold Engineering Development Center, Arnold Airforce Station, TN, February 1978.

6. Taylor, R.P., Coleman, H.W. and Hodge, B.K., "A Discrete Element Prediction Approach for Turbulent Flow Over Rough Surfaces," University of Missippi Report TFD-84-1, February 1984.

7. Schlichting, H., "Boundary Layer Theory," McGraw Hill Book Company, Seventh Edition, 1979.

8. Clauser, F.H., "The Turbulent Boundary Layer," Advances in Applied Mechanics, Vol. IV, Academic Press Inc., 1956, pp. 1-51.

9. Rotta, J., "On the Theory of the Turbulent Boundary Layer," NACA TM 1344, 1953; Translation of "Ueberdie Theorie der Turbulenten Grenzschichten," Mitteilungen aus dem Max-Planck-Institute fur Stromungsforchung, No. 1, 1950.

10. Nikuradse, J., "Stromungsgesetze in Rauhen Rohren," Forsch.-Arbeiten Ing.-Wesen, No. 361, 1933.

11. Goddard, F.E., Jr., "Effects of Uniformly Distributed Roughness on Turbulent Skin Friction Drag at Supersonic Speeds," Journal of the Aeronautical Sciences, Vol. 26, No. 1, January 1959, pp. 1-15.

12. Fenter, F.W., "The Turbulent Boundary Layer on Uniformly Rough Surfaces at Supersonic Speeds," Chance Vaught Research Center Report RE-E9R-2, 1959.

13. Reda, D.C., Ketter, F.C., Jr., and Fan C., "Compressible Turbulent Skin Friction on Rough and Rough/Wavy Walls," AIAA Journal, Vol. 13, No. 5, May 1975, pp. 553-554

14. Schlichting, H., "Experimentelle Untersuchungen Zum Rauhigkeitsproblem," Ing. Archiv, Vol. 7, No. 1 pp. 1-39, 1936.

15. Morris, H.M., "Flow in Rough Conduits," Transaction ASCE, Vol. 120, 1955, p. 373-410.

16. Bettermann D., "Contribution a L'etude de la Convection Force Turbulente le Long de Plaques Rugueuses," International Journal of Heat and Mass Transfer, Vol. 9, No. 3 pp. 153-164, March 1966.

17. Dvorak, F.A., "Calculation of Turbulent Boundary Layers on Rough Surfaces in Pressure Gradient," AIAA Journal, Vol. 7, No. 9, September 1969, pp. 1752-1759.

18. Cebeci, T. and Smith, A.M.O., "Analysis of Turbulent Boundary Layers," Academic Press, 1974.

19. Simpson, R.L., "A Generalized Correlation of Roughness Density Effects on the Turbulent Boundary Layer," AIAA Journal, Vol. 11, No. 2, February 1973, pp. 242-244.

20. Young, A.D. and Paterson, J.H., "Aircraft Excresence Drag," AGARD-AG-264, North Atlantic Treaty Organization, 1981.

21. Dirling, R.B., Jr., "A Method for Computing Roughwall Heat Transfer Rates on Reentry Nose Tips," AIAA Paper No. 73-763, Proceedings of the 8th Thermophysics Conference, Palm Springs, CA, July 1973.

22. Grabow, R.M. and White, C.O., "Surface Roughness Effects on Nosetip Ablation Characteristics," AIAA Journal, Vol. 13, No. 5, May 1975, pp. 605-609.

23. Dalle Donne, M. and Meyer, L., "Turbulent Convective Heat Transfer from Rough Surfaces with Two-Dimensional Rectangular Ribs," International Journal of Heat and Mass Transfer, Vol. 20, No. 6, 1977, pp. 583-620.

24. Coleman, H.W., Hodge, B.K., and Taylor, R.P., "A Re-Evaluation of Schlichting's Surface Roughness Experiment," Journal of Fluid Engineering, Vol. 106, March 1984, pp. 60-65.

25. Webb, R.L., Eckert, E.R.G., and Goldstein, R.J., "Heat Transfer and Friction in Tubes with Repeated Rib Roughness," International Journal of Heat and Mass Transfer, Vol. 14, 1971, pp. 601-617.

26. Han J.C., Glicksman, L.R., and Rohsenow, W.M., "An Investigation of Heat Transfer and Friction for Rib-Roughned Surfaces," International Journal of Heat and Mass Transfer, Vol 21, 1978, pp. 1143-1156.

27. Liu, C.K., Kline, S.J., and Johnston, J.P., "An Experimental Study of Turbulent Boundary Layer on Rough Walls," Department of Mechanical Engineering, Stanford University, Report MD-15, July 1966.

28. Pineau, F., Nguyen, V.D., Dickinson, J., and Belanger, J., "Study of a Flow Over a Rough Surface with Passive Boundary Layer Manipulators and Direct Wall Drag Measurements," AIAA Paper No. 87-0357, 1987.

29. Perry, A.E., and Joubert, P.N., "Rough-Wall Boundary Layers in Adverse Pressure Graidents," Journal of Fluid Mechanics, Vol. 17, 1963, pp. 193-211.

30. Antonia, R.A. and Luxton, R.E., "The Response of a Turbulent Boundary Layer to a Step Change in Surface Roughness, Part 1. Smooth to Rough," Journal of Fluid Mechanics, Vol. 48, Part 4, 1971, pp. 721-762.

31. Antonia, R.A. and Wood, D.H., "Calculation of a Turbulent Boundary Layer Downstream of a Step Change in Surface Roughness," Aeronautical Quarterly, Vol. 26, Part 3, 1975, pp. 202-220.

32. Furuya, Y., Fujita, H., and Nakashima, H., "Turbulent Boundary Layers on Plates Roughned by Wires in Equal Intervals," Data reported by I. Tani in "Perspectives in Turbulence Studies," Springer-Verlag, Berlin, West Germany, 1987, pp. 223-249.

33. Sherif, N. and Gumley, P., "Heat-Transfer and Friction Properties of Surfaces with Discrete Roughnesses," International Journal of Heat and Mass Transfer, Vol. 9, 1966, pp. 1297-1320.

34. Voisinet, R.L.P., "Influence of Roughness and Blowing on Compressible Turbulent Boundary Layer Flow," NSWC-TR-79-153, Naval Surface Weapons Center, White Oak Laboratory, Silver Spring, MD, June 1979.

35. Berg, D.E., "Surface Roughness Effects on a Mach 6 Turbulent Boundary Layer," AIAA Journal, Vol. 17, No. 9, September 1979, pp. 929-930.

36. Brandon, F.J. and Von Whalde, R., "Wind-Tunnel Data for Long Rod, Finned-Stabilized Projectiles," BRL-MR-3618, US Army Ballistic Research Laboratory, Aberdeen Proving Ground, Maryland, 1987.

37. Mason, L.A., Devan, L., Moore, F.G. and McMillan, D., "Aerodynamic Design Manual for Tactical Missiles," NSWC TR-81-156, 1981.

38. Van Driest, E.R., "On Turbulent Flow Near a Wall," Journal of the Aeronautical Sciences, Vol. 23, No. 11, November 1956, p. 1007-1011, 1036.

39. Healzer, J.M., Moffat, R.J. and Kays W.M., "The Turbulent Boundary Layer on a Rough, Porous Plate: Experimental Heat Transfer with Uniform Blowing," Stanford University Report HMT-18, May 1974.

40. Lin, T.C., and Bywater, R.J., "The Evaluation of Selected Turbulence Models for High-Speed Rough-Wall Boundary Layer Calculations," AIAA Paper No. 80-0132, 1980.

41. Han, L.S., "Turbulent Flow Over Rough Turbine Airfoil," Report AFWAL-TR-85-2056, Department of Mechanical Engineering, Ohio State University, August 1985.

42. Schiff, L.B. and Steger, J.L., "Numerical Simulation of Steady Supersonic Viscous Flow," Proceedings of the AIAA 17th Aerospace Sciences Meeting, AIAA Paper No. 79-0130, January 1979.

43. Beam, R. and Warming, R.F., "An Implicit Factored Scheme for the Compressible Navier-Stokes Equations," AIAA Journal, Vol. 16, No. 4, 1978, pp. 85-129.

44. Rai, M.M. and Chaussee, D.S., "New Implicit Boundary Procedures: Theory and Applications," Proceedings of the AIAA 21st Aerospace Science Meeting, AIAA Paper No. 83-0123, January 1983.

45. Baldwin, B.S. and Lomax, H., "Thin Layer Approximation and Algebraic Model for Separated Turbulent Flows," Proceedings of the AIAA 16th Aerospace Sciences Meeting, AIAA Paper No. 78-257, January 1978.

46. Weinacht, P., "Problem in the Computation of the Turbulent Viscosity in Several Versions of MUTUR," Personnel Communication, April 1988.

LIST OF SYMBOLS

a = width, in mainstream direction, of roughness element

A_f = frontal area of a roughness element

A_R = parameter in Healzer model

A_s = windward area of a roughness element

A_∞ = free-stream velocity of sound

C = a constant in the Law of the Wall

C_A = axial-force coefficient

C_{cp}, C_{kleb} = constraints in Baldwin-Lomax turbulence model

C_f = skin friction coefficient

C_{fo} = smooth wall skin friction coefficient

d = average spacing of roughness elements

D = a term in the expression for the change of intercept of the Law of the Wall

D_s = value of D for sand roughness

E = parameter in Han's model

$\hat{E}, \hat{F}, \hat{G}$ = flux vectors in transformed coordinates

G = transition function from smooth to rough

h = height of roughness element

h_{es} = height of equivalent sand roughness

h_s = height of sand roughness

k = Clauser's constant = 0.0168

l = mixing length

M_∞ = free-stream Mach number

p = streamwise spacing of roughness elements

P = pressure

$\hat{q}$ = vectors of dependent variables

R = parameter in Han's model

$\hat{Re}$ = Reynolds number

S = reference area for skin friction, area of smooth surface before adding on the roughness

S_f = total frontal area of roughness elements

S_R = reference area for axial-force coefficient

$\hat{S}$ = viscous source term

u = velocity in mainstream direction

u_e = velocity at the edge of the boundary layer

u_τ = friction velocity

x = longitudinal distance from nose

y = distance from the wall

Greek Symbols

γ = ratio of specific heats

Γ = Klebanoff intermittency factor

κ = Von Karman constant

λ = roughness density parameter, defined in TABLE 1

Λ = composite roughness desity parameter, defined in TABLE 1

μ_t = turbulent viscosity

ν = kinematic viscosity

ξ, η, ζ = transformed coordinates

ρ = density

ω = vorticity

Superscripts

i = inner layer

o = outer layer

r = rough

s = smooth

* = Dalle Donne density parameter

+ = wall parameters

Subscripts

a	=	density parameter base on width
f	=	density parameter based on frontal area
h	=	density parameter based on height
mu	=	math wave
ri	=	start of roughness
s	=	new density parameter
w	=	wall conditions

DISTRIBUTION LIST

No. Copies	Organization
12	Administrator Defense Technical Information Center ATTN: DTIC-DDA Cameron Station Alexandria, VA 22304-6145
1	HQDA (SARD-TR) Washington, DC 20310-0001
1	Commander US Army Material Command ATTN: AMCDRA-ST 5001 Eisenhower Avenue Alexandria, VA 22333-0001
2	Commander Armament RD&E Center U.S. Army AMCCOM ATTN: SMCAR-MSI Picatinny Arsenal, NJ 07806-5000
2	Commander Armament RD&E Center U.S. Army AMCCOM ATTN: SMCAR-TDC Picatinny Arsenal, NJ 07806-5000
1	Commander Benet Weapons Laboratory Armament R&D Center US Army AMCCOM ATTN: SMCAR-LCB-TL Watervliet, NY 12189-4050
1	Director US Army Aviation Research and Technology Activity Moffett Field, CA 94035-1099
1	Commander US Army Communications - Electronics Command ATTN: AMSEL-ED Fort Monmouth, NJ 07703-5022
2	Commander US Army Missile Command ATTN: AMSMI-RD B. Walker Redstone Arsenal, AL 35898-5000
1	Commander US Army Missile Command ATTN: AMSMI-AS Redstone Arsenal, AL 35898-5000
1	Commander US Army Laboratory Command ATTN: AMSLC-DL Adelphi, MD 20783-1145
1	Commander US Army Armament, Munitions and Chemical Command ATTN: SMCAR-ESP-L Rock Island, IL 61299-5000
1	Commander US Army Aviation Systems Command ATTN: AMSAV-DACL 4300 Goodfellow Blvd St Louis, MO 63120-1789

DISTRIBUTION LIST

No. Copies	Organization
1	Commander US Army Tank Automotive Command ATTN: AMSTA-TSL Warren, MI 48397-5000
1	Director US Army TRADOC Analysis Center ATTN: ATAA-SL White Sands Missile Range, NM 88002-5502
1	Dir, Combat Development US Army Infantry School ATTN: ATSH-CD Fort Benning, GA 31905-5660
1	AFWL/SUL Kirtland AFB, NM 87117-5800
2	Commander Naval Surface Weapons Center ATTN: Code R44 (Dr. F. Priolo) Code R44 (Dr. A. Wardlaw) K-24, Building 402-12 White Oak Laboratory Silver Spring, MD 20903-5000
3	Director National Aeronautics and Space Administration Langley Research Center ATTN: Tech Library Mr. P. J. Bobbitt Mr. D. M. Bushnell Dr. M. J. Hemsch Langley Station Hampton, VA 23665
5	Director National Aeronautics and Space Administration Ames Research Center ATTN: MS-227-8, L. Schiff MS-258-1, T. Holst MS-258-1, J. Steger MS-258-1, D. Chaussee MS-258-1, M. Rai MS-229-1 M. Rubesin Moffett Field, CA 94035
5	Commander U.S. Army Armament Research, Development & Engineering Center ATTN: SMCAR-TSS SMCAR-LCA-F J. Grau R. Kline S. Kahn H. Hudgins Picatinny Arsenal, NJ 07806-5000
1	Air Force Armament Laboratory ATTN: AFATL/DLODL Eglin AFB, FL 32542-5000
2	United States Military Academy Department of Mechanics ATTN: LTC Andrew L. Dull LTC Thomas Kiehne West Point, NY 10996

DISTRIBUTION LIST

No. Copies	Organization
1	Massachusetts Institute of Technology ATTN: Tech Library 77 Massachusetts Avenue Cambridge, MA 02139
1	Commander US Naval Surface Weapons Center ATTN: Dr. F. Moore Dahlgren, VA 22448
1	Air Force Armament Laboratory ATTN: AFATL/FXA (Stephen C. Korn) Eglin AFB, FL 32542-5434
1	AEDC Calspan Field Service ATTN: MS 600 (Dr. John Benek) AAFS, TN 37389
1	Virginia Polytechnic Institue & State University ATTN: Dr. Clark H. Lewis Department of Aerospace & Ocean Engineering Blacksburg, VA 24061
1	University of California, Davis Department of Mechanical Engineering ATTN: Prof. H.A. Dwyer Davis, CA 95616
1	Pennsylvania State University Department of Aerospace Engineering ATTN: Dr. G. S. Dulikravich University Park, PA 16802
1	University of illinois at Urbana Champaign Department of Mechanical and Industrial Engineering Urbana, IL 61801
1	University of Maryland Department of Aerospace Engr. ATTN: Dr. J. D. Anderson, Jr. College Park, MD 20742
1	University of Notre Dame Department of Aeronautical and Mechanical Engineering ATTN: Prof. T. J. Mueller Notre Dame, IN 46556
1	University of Texas Department of Aerospace Engeering and Engineering Mechanics ATTN: Dr. D. S. Dolling Austin, Texas 78712-1055
1	University of Delaware Department of Mechanical Engineering ATTN: Dr. John Meakin Chairman Newark, DE 19716
1	University of Florida Department of Engineering Sciences College of Engineering ATTN: Prof. C. C. Hsu Gainesville, FL 32611

DISTRIBUTION LIST

No. Copies	Organization
2	USAF Wright Aeronautical Laboratories ATTN: AFWAL/FIMG Mr. Norman E. Scaggs Dr. J. Shang WPAFB, OH 45433-6553
1	Grumann Aerospace Corporaton Aerophysics Research Department ATTN: Dr. R. E. Melnik Bethpage, NY 11714
1	Advanced Technology Center Arvin/Calspan Aerodynamics Research Department ATTN: Dr. M. S. Holden P. O. Box 400 Buffalo, NY 14225
1	Analytical Methods, Inc. ATTN: Mr. F. A. Dvorak 2047 152nd Ave., N.E. Redmond, WA 98052
2	David Taylor Research Center ATTN: Dr. P. S. Granville Dr. de los Santos Bethesda, MD 20084
1	Physical Science Inc. ATTN: Dr. M. L. Finson Research Park Andover, MA 01810
2	Director Sandia National Laboratories ATTN: Dr. W. Oberkampf Dr. F. Blottner Division 1636 Albuquerque, NM 87185
1	The University of Arizona Aerospace Engineering Department ATTN: Prof. I. Wygnanski Tucson, AZ 85721
1	Applied Technology Associates ATTN: Mr. R. J. Cavalleri P.O. Box 19434 Orlando, FL 32814
1	United Technologies Corporation Chemical Systems Division ATTN: Mr. A. L. Holzman P.O. Box 50015 600 Metcalf Road San Jose, CA 95150-0015
1	Ford Aerospace and Communications Corporation Aeronutronnics Division ATTN: Charles White Bud Blair Ford Road Newpoint Beach, CA 92658
1	Honeywell Inc. ATTN: Wilford E. Martwick Ken Sundeen 600 Second Street, North East Hopkins, MN 55343
1	University of Cincinnati Department of Aerospace Engineering ATTN: Prof. Stanley Rubin Mail Location 70 Cincinnati, OH 45221

DISTRIBUTION LIST

No. Copies	Organization	No. Copies	Organization
1	Illinois Institute of Technology College of Engineering Fluid Dynamics Research Center ATTN: Dr. Mukund Acharya IIT Center Chicago, IL 60616		

Aberdeen Proving Ground

Director, USAMSAA
ATTN: AMXSY-D
AMXSY-MP, H. Cohen

Commander, USATECOM
ATTN: AMSTE-TO-F

Cdr, CRDC, AMCCOM
ATTN: SMCCR-MU
SMCCR-RSP-A
SMCCR-SPS-IL